

2

WGL-114-001-044
KSS-10

LARGE DEFLECTION ELASTIC-PLASTIC DYNAMIC RESPONSE OF STIFFENED SHELLS OF REVOLUTION

DRA

aerospace engineering department



TEXAS A&M UNIVERSITY

James A. Stricklin, Walter E. Haisler, .
Walter A. Von Riesemann, Roger D. Leick,
Barry Hunsaker and Kenneth J. Saczalski

(NASA-CR-132044) LARGE DEFLECTION
ELASTIC-PLASTIC DYNAMIC RESPONSE OF
STIFFENED SHELLS OF REVOLUTION (Texas A&M
Univ.) 113 p HC \$7.75 CSCL 20K
108

N73-24902
Unclas
17628

G3/32

December 1972

TEXAS ENGINEERING EXPERIMENT STATION

Large Deflection Elastic-Plastic Dynamic Response
of Stiffened Shells of Revolution

James A. Stricklin,* Walter E. Haisler,*
Walter A. Von Riesemann,** Roger D. Leick,*
Barry Hunsaker,* and Kenneth J. Saczalski***

December 1972

*Aerospace Engineering Department, Texas A&M University, College Station, Texas

**Staff Member, Sandia Laboratories, Albuquerque, New Mexico

***Structural Mechanics Program, Office of Naval Research, Arlington, Virginia

Acknowledgement

This Research was supported under Sandia Laboratories Contract 82-7739, Navy Contract N00011-68-A-0308-0004, and NASA Grant NGL-44-001-044. Appreciation is expressed to Dr. Fred Stebbins of the Manned Spacecraft Center, Houston, Texas, who served as technical monitor on the NASA Grant.

Appreciation is also expressed to Dr. N. J. Huffington, Jr. of Ballistic Research Laboratories, Aberdeen Proving Ground, Maryland, for furnishing many of the check out problems.

Abstract

This report presents the formulation and check out problems for a computer code DYNAPLAS, which analyzes the large deflection elastic-plastic dynamic response of stiffened shells of revolution. The formulation for special discretization is by the finite element method with finite differences being used for the evaluation of the pseudo forces due to material and geometric nonlinearities. Time integration is by the Houbolt method. The stiffeners may be due to concentrated or distributed eccentric rings and spring supports at arbitrary angles around the circumference of the elements. Check out problems include the comparison of solutions from DYNAPLAS with experimental and other computer solutions for rings, conical and cylindrical shells and a curved panel. A hypothetical submarine including stiffeners and missile tube is studied under a combination of hydrostatic and dynamically applied asymmetrical pressure loadings.

Table of Contents

| | |
|---|-----|
| Acknowledgement | ii |
| Abstract | iii |
| Table of Contents | iv |
| List of Figures | vi |
| Nomenclature | vii |
| Introduction | 1 |
| Formulation | 6 |
| Plasticity Relations | 12 |
| Isotropic Hardening | 13 |
| Kinematic Hardening | 15 |
| Comparison of Isotropic and Kinematic Hardening | 18 |
| Solution Procedure | 19 |
| Shell of Revolution | 22 |
| Strain Displacement Relations | 23 |
| Linear Stiffness Matrix | 24 |
| Mass Matrix | 25 |
| Nonlinear Terms | 25 |
| Ring Stiffeners | 29 |
| Spring Supports | 31 |
| Computational Procedure | 34 |
| Computer Programs | 37 |
| Check Out Problems | 42 |
| Static Solution for Spherical Cap | 42 |
| Symmetrically Impulsively Loaded Ring | 43 |
| Free Ring Under Half-Cosine Impulsive Load | 44 |
| Clamped Ring Under Impulsive Loading | 45 |
| Cylindrical Shell Under Impulsive Load | 47 |
| Circular Plate Under Impulsive Load | 48 |
| Truncated Cone Under Half-Cosine Impulse | 49 |
| Cylinder Under Moving Pressure Load | 51 |
| Conical Frustum Under Half-Cosine Impulse | 54 |
| Hypothetical Submarine | 55 |
| Cylindrical Panel | 58 |

v

| | |
|------------------------|-----|
| Users Hints | 59 |
| Extensions in Progress | 60 |
| Statement of Policy | 61 |
| References | 62 |
| Appendix A | 95 |
| Distribution List | 100 |

List of Figures

- 1 Directions of Kirchhoff Stress
- 2 Center Deflection Vs Time for Circular Plate
- 3 Dynamic Response of Simple Mass
- 4 Generalized Coordinates of Shell Element
- 5 Support on Cylindrical Ring
- 6 Meridional Bending Moment vs. Angle From
Apex for a Spherical Cap
- 7 Radial Displacement for Various Values of
the Strain-Hardening Parameter, λ
- 8 Radial Displacement At $\theta = 0^\circ$
- 9 Plastic Strain at Outer Surface and $\theta = 0^\circ$
Versus Time
- 10 Radial Displacement at $\theta = 0.0^\circ$
- 11 Circumferential Strain at $\theta = 0.0^\circ$ on
the Outer Surface
- 12 Rotation of a Clamped Ring
- 13 Radial Displacement Around the Circumference
at $L/2$
- 14 Center Deflection vs Time for an Impulsively
Loaded Circular Plate
- 15 Meridional Strain on Top at Radius of 2.125 in
- 16 Axial and Radial Displacement For $\theta = 0^\circ$
and $Z=6.3516$ inches
- 17 Axial and Circumferential Strain at $\theta = 0^\circ$
and $Z=6.3516$ in (Outer Surface)
- 18 Axial and Circumferential Strain at $\theta = 0^\circ$
and $Z=6.3516$ in (Inner Surface)
- 19 Deflection at $\theta = 0^\circ$ and $Z = L/2$ For a Cylinder
Subjected to a Moving Pressure Load
- 20 Midsurface Axial Strain at $\theta = 0^\circ$ and
 $Z = L/2$ For a Cylinder Subjected to a
Moving Pressure Load
- 21 Radial Deflection at $\theta = 0.0^\circ$ and
 $Z=6.3516$ inches
- 22 Meridional and Circumferential Strain at
 $\theta = 0$ and $Z=6.3516$ inches
(Inner Surface)
- 23 Meridional and Circumferential Strain at
 $\theta = 00^\circ$ and $Z=6.3516$ in (Outer Surface)
- 24 Stiffened Cylindrical Shell With Hemispherical
Endcaps and Diametrical Tubes
- 25 Element Idealization of Stiffened Shell
- 26 Meridional Strain at $\theta = 0.0^\circ$ at Missile
Tube, Outer Surface
- 27 Radial Deflection of Node 46 with Respect to
Node 1 for Harmonic 1

Nomenclature

| | |
|---------|--|
| L | = row matrix |
| $\{ \}$ | = column matrix |
| $[]$ | = square matrix |
| C | = coefficients in Eq. 63 |
| $[D]$ | = matrix relating stress to elastic strain |
| E | = Young's Modulus |
| e | = linear expressions for midsurface strains and rotations |
| f | = force unbalance in equation of equilibrium |
| H' | = slope of uniaxial stress vs. uniaxial plastic strain |
| I | = area moment of inertia |
| $[K]$ | = matrix of stiffness coefficients |
| L | = meridional length of element |
| $[M]$ | = mass matrix |
| m | = number of subincrements used in computing plastic strain increment |
| N | = number of circumferential stiffeners per element |
| P | = applied external loads |
| Q | = pseudo forces due to nonlinearities |
| q | = generalized coordinates |
| r | = radial distance to midsurface of shell |
| S | = Kirchhoff stress |
| s | = meridional distance |
| t | = thickness of shell element and time |
| u | = displacements |

| | |
|------------------|---|
| V | = undeformed volume |
| v | = circumferential displacement |
| W | = potential due to applied and inertia forces |
| w | = displacement normal to shell |
| z | = distance from midsurface of shell |
| α | = translation of yield surface |
| Δ | = increment |
| ϵ | = strain |
| $\bar{\epsilon}$ | = equivalent uniaxial value of strain |
| θ | = circumferential angle |
| χ | = changes in curvature |
| ρ | = mass density |
| σ | = stress |
| ϕ | = slope of undeformed shell |

Superscripts and Subscripts

| | |
|----------|---|
| e | = elastic contribution |
| I | = initial strain contribution |
| i | = time increment, degree of freedom, dummy summation variable |
| j | = degree of freedom, summation index |
| L | = contribution based on linear theory |
| NL | = contribution due to geometric nonlinearities |
| o | = initial value |
| P | = contribution due to plastic strains |
| s | = meridional direction and springs |
| θ | = circumferential direction |

INTRODUCTION

Due primarily to advances in computer technology the analysis of the large deflection elastic-plastic response of realistic structures is now within the realm of reality. Several computer codes have already been developed for this purpose. These include finite difference codes by the groups at M.I.T.,^{2,3} Ballistic Research Laboratories,^{23,24,25} Sandia Laboratories,^{8,32} and Lockheed.^{57,61} Finite element computer codes have been developed by McNamara and Marcal,³⁶ Wu and Witmer,⁶² and Stricklin et al.⁴⁹ In general all the codes have certain limitations. The finite difference codes are generally restricted to unstiffened shells whereas the finite element codes do not have this restriction but are restricted to simple structures. There is a need for a code to analyze the large deflection elastic-plastic deformation of stiffened shells of revolution.

Basically there are three different formulations which have been used in the analysis of the nonlinear behavior of structures. The first formulation treats the effects of nonlinearities as pseudo forces on the right hand side of the equations of equilibrium. This formulation requires that only pseudo forces be computed but has the disadvantage of the occurrence of numerical stability problems when certain solution procedures are employed. The basic equations of equilibrium neglecting damping, for this method are derived in detail in this report and symbolically may be written as

$$[M]\{\ddot{q}\} + [K]\{q\} = \{P\} + \{Q^I\} + \{Q^{NL}\} \quad (1)$$

where

$[M]$ = mass matrix

$[K]$ = stiffness matrix

$\{q\}$ = generalized displacement

$\{P\}$ = generalized forces due to applied loads

$\{Q^I\}$ = pseudo forces due to initial (plastic) strains

$\{Q^{NL}\}$ = pseudo forces due to geometric nonlinearities

Farhoomand and Wilson¹⁶ and McNamara and Marcal³⁶ use the incremental form of Eq. 1 for their formulation. This is obtained as follows, first Eq. 1 is written in incremental form:

$$[M]\{\Delta\ddot{q}\} + [K]\{\Delta q\} = \{\Delta P\} + \{\Delta Q^I\} + \{\Delta Q^{NL}\} \quad (2)$$

next the increments of Q^I and Q^{NL} are treated as differentials and evaluated by applying the chain rule in terms of the generalized displacements q_i .

$$\Delta Q_i^I = \frac{\partial Q_i^I}{\partial q_j} \Delta q_j = -K_{ij}^I \Delta q_j \quad (3)$$

$$\Delta Q_i^{NL} = + \frac{\partial Q_i^{NL}}{\partial q_j} \Delta q_j = -K_{ij}^{NL} \Delta q_j$$

Using the relations given by Eq. 3, Eq. 2 becomes

$$[M]\{\Delta\ddot{q}\} + ([K] + [K^I] + [K^{NL}])\{\Delta q\} = \{\Delta P\} + \{f_0\} \quad (4)$$

where the unbalance in force $\{f_0\}$ has been added to the right hand side as was done in Refs. 18 and 36.

A new and completely different formulation is presented by Wu and Witmer.⁶² Starting with the virtual work expression in terms of stress and increments of strain, Wu and Witmer obtained the equilibrium equations in the form:

$$[M]\{\ddot{q}\} + \{\bar{P}\} + [H]\{q\} = \{F\} \quad (5)$$

In Eq. 5, $\{F\}$ represents the generalized forces due to external loads. The matrices $\{\bar{P}\}$ and $[H]$ depend on the state of stress in the body.

It is difficult to state the relative advantages and disadvantages of the formulations given by Eqs. 1, 4, and 5, respectively. However for the asymmetric deflection of shells of revolution where the displacements in the circumferential direction are represented by Fourier series the representation given by Eq. 1 is superior. This is due to the coupling between Fourier terms which appears in $[K^I]$, $[K^{NL}]$, and $[H]$ in Eqs. 4 and 5. This coupling, for all practical purposes, eliminates the possibility of using implicit solution procedures for the formulation given by Eqs. 4 and 5.

Regarding solution procedures it should be noted that there is no solution procedure which may be designated as "The Solution Procedure" due to the dependence of solution procedures on the problem under consideration. The objective here is to discuss several solution procedures in general and devote special emphasis to the formulation given by Eq. 1 as applied to shells of revolution.

The central difference solution procedure for the time response has long been the favorite of researchers using a finite difference formulation of the spatial derivatives.

More recently, central differences have been used in conjunction with the finite element method by Wu and Witmer,⁶² Key and Beisinger,²⁸ and Krieg and Key.³³ The general consensus reached by these researchers is that the central difference solution procedure should be used in conjunction with the "lumping" of masses at the nodes. Further, Key and Beisinger have presented a rational method for lumping the rotary inertia.

Undoubtedly the central difference or some other explicit solution procedure becomes quite attractive as the band width of the stiffness matrix becomes reasonably large. It should be pointed out, however, that the use of conditionally stable procedures is somewhat a contradiction of the basic philosophy of the finite element method. One of the advantages of the finite element approach is that the size of the elements may vary and small elements may be used in regions where the stress gradient is large. However, the time increment which may be used is determined by the highest represented frequency of the system which in turn is increased by using very small elements. Thus, the time increment for numerical stability may become so small as to be of little practical value when very small elements are used. This was indeed found to be the case in Ref. 49 for shells of revolution.

There are three implicit solution procedures which have received considerable attention. They are the Houbolt,²¹ Newmark Beta method,⁴² and Wilson⁶ solution procedures. They are similar in that the matrix which must be "inverted" is a combination of the mass and stiffness matrix. For linear problems the Houbolt procedure is unconditionally stable whereas the Newmark Beta method and Wilson procedures are stable for a certain

range of parameters.

Bathe and Wilson⁶ and Nickell⁴³ have presented interesting studies of the three methods and have shown that the artificial damping is equivalent to conducting an analysis through modal superposition with the higher modes being suppressed. They also present some interesting figures showing what time increment must be chosen to prevent excessive damping or phase shifts. Nickell also presents a discussion of the solution of non-linear problems but no numerical examples are presented.

The authors' experiences with the Houbolt and Newmark Beta procedures are reported in Ref. 54 but are worthy of a summary herein. A particular form of the Newmark Beta method, commonly referred to as the method of Chan, Cox, and Benfield,¹⁰ was used to solve many problems in Ref. 54. It was found that both procedures are no longer unconditionally stable when geometric nonlinearities are included. However, the Houbolt method was found to be considerably more stable than the method of Chan, Cox, and Benfield. In both methods the pseudo forces on the right hand side were determined based on a linear extrapolation; but it was found that the method of Chan, Cox, and Benfield becomes unstable even if the pseudo forces are used as their values at the previous time increment. Another general conclusion which may be reached from the results presented in Ref. 54 is that it is extremely risky to draw conclusions about a non-linear analysis based on a study of the linear problem. The same reasoning works in reverse as the method of Chan, Cox, and Benfield is superior to the Houbolt method for linear problems.

In the present research the Houbolt solution procedure is used although it is planned to permit an option of either the Houbolt or Newmark Beta Methods in the future. The Houbolt method was selected for economic reasons but results presented herein show that the method is quite accurate. The artificial damping in the Houbolt method permits the use of the economical formulation given by Eq. 1 and further permits the pseudo force terms to be extrapolated without appreciable loss in accuracy.

FORMULATION

There are two basic formulations which have been used in nonlinear analysis by the finite element method. The first is the Lagrangian formulation and the other is the use of an incremental moving coordinate system. The three formulations discussed in the introduction which includes the one used herein are of the Lagrangian type. The basic starting point for the formulation is the equations of equilibrium written in terms of the Kirchhoff stress¹⁷ (Fig. 1).

$$\frac{\partial}{\partial a_j} [S_{jk}(\delta_{ik} + \frac{\partial u_i}{\partial a_k})] + \rho_0 F_{oi} = \rho_0 \ddot{u}_i \quad (6)$$

where

S_{jk} = Kirchhoff stress tensor

a_i = coordinate in original body

u_i = Lagrangian displacement

$\rho_0 F_{oi}$ = body force

δ_{ik} = Kronecker delta

\ddot{u} = acceleration

Multiplying Eq. 6 by a virtual displacement δu_i (index summation noted) and integrating over the undeformed body yields the equations of equilibrium in the form

$$\int_{V_0} \rho_0 \ddot{u}_i \delta u_i dV + \int_{V_0} [S] \{\delta \epsilon\} dV = \delta W^* \quad (7)$$

where

$[S]$ = 1 x 6 matrix of Kirchhoff stresses

$\{\epsilon\}$ = 6 x 1 matrix of Green or Lagrangian strains

$$\epsilon_{ij} = \frac{\partial u_i}{\partial a_j} + \frac{\partial u_j}{\partial a_i} + \frac{\partial u_k}{\partial a_i} \frac{\partial u_k}{\partial a_j} \quad i \neq j \quad (8)$$

$$\epsilon_{ij} = \frac{\partial u_i}{\partial a_j} + \frac{1}{2} \frac{\partial u_k}{\partial a_i} \frac{\partial u_k}{\partial a_j} \quad i = j$$

δW^* = virtual work done in deformed body

V_0 = volume of undeformed body

The derivation of Eq. 7 from Eq. 6 follows exactly the same procedure as for the small deflection case presented by Argyris.¹ Obtaining the virtual work in the deformed body, δW^* , requires a physical interpretation of the Kirchhoff stress tensor as presented in Novozhilov⁴⁵ and, in more detail, by Haisler.¹⁸

Restricting attention to small strains, the Kirchhoff stress is the true stress and is related to the elastic component of the Green

strains through the matrix [D]

$$\{S\} = [D]\{\epsilon^e\} \quad (9)$$

As small strains are assumed the total strain is the linear superposition of the various components.

$$\{\epsilon\} = \{\epsilon^e\} + \{\epsilon^P\} + \{\epsilon^T\} + \dots \quad (10)$$

Solving Eq. 10 for the elastic strain, substituting into Eq. 9, and substituting the result into Eq. 7 yields:

$$\int_{V_0} \rho_0 \ddot{u}_i \delta u_i dV + \int_{V_0} ([\epsilon] - [\epsilon^P] - [\epsilon^T] - \dots)[D]\{\delta\epsilon\} = \delta W^* \quad (11)$$

For some problems the potential due to external forces may be a higher order function of the displacements; but, as usual, the assumption of a first order function of the displacements is assumed herein.

$$W^* = [q]\{P(t)\} \quad (12)$$

Thus

$$\delta W^* = [P]\{\delta q\} \quad (13)$$

Taking the variation with respect to generalized coordinate q_i yields the equation of equilibrium:

$$\int_{V_0} \rho_0 \ddot{u}_j \frac{\partial u_j}{\partial q_i} dV + \int_{V_0} \left[\frac{\partial \epsilon}{\partial q_i} \right] [D]\{\epsilon\} dV - \int_{V_0} \left[\frac{\partial \epsilon}{\partial q_i} \right] [D]\{\epsilon^P\} dV - \int_{V_0} \left[\frac{\partial \epsilon}{\partial q_i} \right] [D]\{\epsilon^T\} dV - \dots = \{P\} \quad (14)$$

It is convenient to write the total strain as

$$\epsilon = \epsilon_L + \epsilon_{NL} \quad (15)$$

where ϵ_L and ϵ_{NL} are the linear and nonlinear contributions, respectively, to the total strain. Substituting Eq. 15 into Eq. 14 and expanding the second term on the left hand side, yields

$$\begin{aligned} \int_{V_0} \rho_0 \ddot{u}_j \frac{\partial u_j}{\partial q_i} dV + \int_{V_0} \left[\frac{\partial \epsilon_L}{\partial q_i} \right] [D] \{\epsilon_L\} dV + \int_{V_0} \left[\frac{\partial \epsilon}{\partial q_i} \right] [D] \{\epsilon_{NL}\} dV \\ + \int_{V_0} \left[\frac{\partial \epsilon_{NL}}{\partial q_i} \right] [D] \{\epsilon_L\} dV - \int_{V_0} \left[\frac{\partial \epsilon}{\partial q_i} \right] [D] \{\epsilon^P\} dV \quad (16) \\ - \int_{V_0} \left[\frac{\partial \epsilon}{\partial q_i} \right] [D] \{\epsilon^T\} dV - \dots = P_i \end{aligned}$$

The first term in Eq. 16 produces the terms of the mass matrix times the accelerations. The second term gives the contribution to the usual linear stiffness matrix times the generalized coordinate. The remaining terms may be combined to yield

$$\begin{aligned} m_{ij} \ddot{q}_j + k_{ij} q_j = P_i - \int_{V_0} \left[\frac{\partial \epsilon_{NL}}{\partial q_i} \right] [D] \{\epsilon_L\} \\ - \int_{V_0} \left[\frac{\partial \epsilon}{\partial q_i} \right] [D] \{\epsilon_{NL} - \epsilon^P - \epsilon^T - \dots\} dV \quad (17) \end{aligned}$$

where

$$m_{ij} = \int_{V_0} \rho_0 \frac{\partial u_l}{\partial q_i} \frac{\partial u_l}{\partial q_j} dV \quad (18)$$

$$k_{ij} = \int_{V_0} \left[\frac{\partial \epsilon_L}{\partial q_i} \right] [D] \left\{ \frac{\partial \epsilon_L}{\partial q_j} \right\} dV \quad (19)$$

It should be noted that the volume integrals extend over the entire region affected by q_i and q_j . This integration is, of course, performed by integrating over each element separately and assembling the results in the standard manner.

Writing Eq. 17 for each and every degree of freedom yields the complete set of equilibrium equations in matrix form.

$$[M]\{\ddot{q}\} + [K]\{q\} = \{P\} + \{Q^*\} \quad (20)$$

where

$$Q_i^* = - \int_{V_0} \left[\frac{\partial \epsilon_{NL}}{\partial q_i} \right] [D] \{\epsilon_L\} dV - \int_{V_0} \left[\frac{\partial \epsilon}{\partial q_i} \right] [D] \{\epsilon_{NL} - \epsilon^P - \epsilon^T \dots\} dV \quad (21)$$

The last term on the right side of Eq. 20 is generally called the pseudo force and is a function of the unknown displacements.

In Eq. 21 the pseudo forces due to material and geometric nonlinearities are included together instead of separating them into components. The separate components are given as:

$$Q_i^* = Q_i^I + Q_i^{NL} \quad (22)$$

where

Q_i^I = pseudo force due to initial (plastic) strains

Q_i^{NL} = pseudo force due to geometric nonlinearities

$$Q_i^I = \int_{V_0} \left[\frac{\partial \epsilon}{\partial q_i} \right] [D] \{ \epsilon^P + \epsilon^T + \dots \} dV \quad (23)$$

$$Q_i^{NL} = - \int_{V_0} \left[\frac{\partial \epsilon_{NL}}{\partial q_i} \right] [D] \{ \epsilon_L \} dV - \int_{V_0} \left[\frac{\partial \epsilon}{\partial q_i} \right] [D] \{ \epsilon_{NL} \} dV \quad (24)$$

$$= - \int_{V_0} \left[\frac{\partial \epsilon_L}{\partial q_i} \right] [D] \{ \epsilon_{NL} \} dV - \int_{V_0} \left[\frac{\partial \epsilon_{NL}}{\partial q_i} \right] [D] \{ \epsilon \} dV$$

The last form of Eq. 24 is the more efficient from the computational point of view when only geometric nonlinearities are considered. Furthermore, within the realm of shell analysis Eq. 24 may be integrated through the thickness of the shell. The approximate expressions, assuming moderate rotations, for total strain in the shell with the ring stiffener being a special case is given by:

$$\{ \epsilon \} = \{ e \} + \{ \epsilon_{NL} \} + z \{ \kappa \} \quad (25)$$

where

$\{ e \}$ are the usual expressions for the linear membrane strains

$\{ \kappa \}$ are the changes in curvature and twist

and z is the distance from the reference surface.

Substituting Eq. 25 into the second form of Eq. 24 and integrating through the thickness yields

$$Q_i^{NL} = -t \int_{A_0} \left[\frac{\partial e}{\partial q_i} + \bar{z} \frac{\partial \kappa}{\partial q_i} \right] [D] \{ \epsilon_{NL} \} dA$$

$$- t \int_{A_0} \left[\frac{\partial \epsilon_{NL}}{\partial q_i} \right] [D] \{ e + \epsilon_{NL} + \bar{z} \kappa \} dA$$
(26)

where t is the thickness and \bar{z} is the distance from the reference surface to the centroid of the area under consideration. In the present research it is assumed that the midsurface of the shell is the reference surface and thus \bar{z} for the shell is zero. But, the circumferential stiffeners may be eccentrically located which gives a non-zero value for \bar{z} .

The basic governing equations are Eqs. 20, 23, and 26 and these equations should be discussed. First from Eq. 23 it should be observed that the pseudo forces due to initial strain are functions of the displacement and hence vary with time (ϵ_{NL} is a second order function of the displacements). Next it should be observed that the formulation to this point is valid for any type of shell. Specialization of the formulation to the shell of revolution and ring stiffeners is presented in a later section.

PLASTICITY RELATIONS

The Von Mises yield condition and isotropic hardening are used in the present study. However, this section includes a discussion of kinematic hardening as well as isotropic hardening. The presentation for

isotropic hardening follows that given by Marcal.³⁸ All discussions are for the plane stress case.

Isotropic Hardening

The expression for the equivalent uniaxial stress is given by

$$\bar{\sigma} = [\sigma_s^2 + \sigma_\theta^2 - \sigma_s \sigma_\theta + 3\sigma_{s\theta}^2]^{1/2} \quad (27)$$

where s and θ are the meridional and circumferential directions respectively. Elastic behavior is observed if $\bar{\sigma}$ is less than the yield stress in uniaxial tension. The normality condition for the increment of plastic strain is:

$$\{d\epsilon^P\} = d\bar{\epsilon}^P \left\{ \frac{\partial \bar{\sigma}}{\partial \sigma} \right\} \quad (28)$$

where

$\{d\epsilon^P\}$ = increment of plastic strain

$d\bar{\epsilon}^P$ = increment of equivalent uniaxial plastic strain.

The hardening rule for the material is simply the relation between the uniaxial plastic strain increment $d\bar{\epsilon}^P$ and the uniaxial stress increment.

$$d\bar{\sigma} = H' d\bar{\epsilon}^P \quad (29)$$

For any type of stress strain curve

$$H' = \frac{E E_T}{E - E_T} \quad (30)$$

where

E_T = tangent modulus

E = Young's modulus

The other relation needed to complete the formulation is the equation relating the increment of stress to the increment of elastic strain.

$$\{\mathrm{d}\sigma\} = [D]\{\mathrm{d}\varepsilon^e\} = [D](\{\mathrm{d}\varepsilon\} - \{\mathrm{d}\varepsilon^P\}) \quad (31)$$

Premultiplying Eq. 31 by $[\frac{\partial \bar{\sigma}}{\partial \sigma}]$ and using Eqs. 28 and 29 yields:

$$[\frac{\partial \bar{\sigma}}{\partial \sigma}] \{\mathrm{d}\sigma\} = \mathrm{d}\bar{\sigma} = H' \mathrm{d}\varepsilon^P = [\frac{\partial \bar{\sigma}}{\partial \sigma}] [D] (\{\mathrm{d}\varepsilon\} - \mathrm{d}\varepsilon^P \{\frac{\partial \bar{\sigma}}{\partial \sigma}\}) \quad (32)$$

Solving Eq. 32 for $\mathrm{d}\varepsilon^P$ yields:

$$\mathrm{d}\varepsilon^P = \frac{[\frac{\partial \bar{\sigma}}{\partial \sigma}] [D] \{\mathrm{d}\varepsilon\}}{H' + [\frac{\partial \bar{\sigma}}{\partial \sigma}] [D] \{\frac{\partial \bar{\sigma}}{\partial \sigma}\}} \quad (33)$$

In the computational procedure the equivalent uniaxial strain given by Eq. 33 is first computed and then the increments of plastic strain and stress are computed through Eqs. 28 and 31 respectively. When the equivalent uniaxial strain computed by Eq. 33 is less than zero unloading occurs and $\mathrm{d}\varepsilon^P$ is set equal to zero.

The treatment of the transition range from elastic to plastic behavior follows the same procedure given by Krieg and Duffey³² and Yamada et.al.⁶⁴

It was found during the course of preliminary research in this area that the straight-forward computational procedure presented here can, if large increments of strain occur, yield stresses which deviate appreciably from the assumed stress-strain curve. To avoid this deviation the strain increment in Eq. 33 is divided into m sub-increments and the procedure

repeated for each sub-increment. The stresses are updated in each sub-increment which gives modified values for the direction normal to the yield surface $[\frac{\partial \bar{\sigma}}{\partial \sigma}]$. The number of sub-increments is determined by computing an equivalent uniaxial strain increment, using the relation for equivalent uniaxial plastic strain, and dividing by an allowable increment of strain. Thus the number of sub-increments varies with time and position on the structure.

The storage requirements for the implementation of isotropic hardening are the three plastic strain arrays, the uniaxial plastic strain array, and the maximum stress array. The uniaxial plastic strain is needed to determine H' whereas the maximum stress must be exceeded after unloading before additional plastic straining occurs.

Kinematic Hardening

The form of kinematic hardening presented here is based on Ziegler's modification of Prager's hardening rule.⁶⁵ Much of the derivation of kinematic hardening follows the same procedure used for isotropic hardening; but is presented here for completeness.

The yield condition for kinematic hardening is given by:

$$\bar{\sigma} = [(\sigma_s - \alpha_s)^2 + (\sigma_\theta - \alpha_\theta)^2 - (\sigma_s - \alpha_s)(\sigma_\theta - \alpha_\theta) + 3(\sigma_{s\theta} - \alpha_{s\theta})^2]^{1/2} \quad (34)$$

where the α 's represent the translation of the yield surface. Yielding occurs whenever $\bar{\sigma}$ is greater than the yield stress in uniaxial tension.

The flow rule for kinematic hardening is, as in isotropic hardening, the normality condition.

$$\{d\epsilon^P\} = d\epsilon^{-P} \left\{ \frac{\partial \bar{\sigma}}{\partial \sigma} \right\} \quad (35)$$

The hardening rule is the one given by Prager

$$[d\sigma - H' d\epsilon^P] \left\{ \frac{\partial \bar{\sigma}}{\partial \sigma} \right\} = 0 \quad (36)$$

where H' is again given by Eq. 30.

The stress increment is again determined by the elastic strain increment through the matrix $[D]$.

$$\{d\sigma\} = [D]\{d\epsilon^E\} = [D](\{d\epsilon\} - \{d\epsilon^P\}) \quad (37)$$

Substituting Eq. 35 into Eq. 36 and taking the transpose of the resulting equation yields

$$\left[\frac{\partial \bar{\sigma}}{\partial \sigma} \right] \{d\sigma\} = \left[\frac{\partial \bar{\sigma}}{\partial \sigma} \right] \left\{ \frac{\partial \bar{\sigma}}{\partial \sigma} \right\} H' d\epsilon^{-P} \quad (38)$$

Also using Eq. 35 in Eq. 37 and premultiplying by $\left[\frac{\partial \bar{\sigma}}{\partial \sigma} \right]$ yields:

$$\left[\frac{\partial \bar{\sigma}}{\partial \sigma} \right] \{d\sigma\} = \left[\frac{\partial \bar{\sigma}}{\partial \sigma} \right] [D] (\{d\epsilon\} - d\epsilon^{-P} \left\{ \frac{\partial \bar{\sigma}}{\partial \sigma} \right\}) \quad (39)$$

Solving Eqs. 38 and 39 for $d\epsilon^{-P}$ yields:

$$d\epsilon^{-P} = \frac{\left[\frac{\partial \bar{\sigma}}{\partial \sigma} \right] [D] \{d\epsilon\}}{\left[\frac{\partial \bar{\sigma}}{\partial \sigma} \right] ([H' \quad] + [D]) \left\{ \frac{\partial \bar{\sigma}}{\partial \sigma} \right\}} \quad (40)$$

The diagonal matrix $[H']$ has been inserted for convenience in computation. The similarity between Eq. 40 and Eq. 33 should be observed. Using kinematic hardening Eqs. 40, 35, and 37 form the basic equations; however,

these equations must be supplemented by an equation which yields the increments in α_s , α_θ , and $\alpha_{s\theta}$. This equation is the primary modification made by Ziegler and is given by:

$$\{d\alpha\} = d\mu \{\sigma - \alpha\} \quad (41)$$

The term $d\mu$ which must be greater than zero is determined by noting that the yield surface translates but does not enlarge. Thus:

$$d\bar{\sigma} = \left[\frac{\partial \bar{\sigma}}{\partial \sigma} \right] \{d\sigma\} + \left[\frac{\partial \bar{\sigma}}{\partial \alpha} \right] \{d\alpha\} = 0 \quad (42)$$

Examination of Eq. 34 reveals that

$$\left\{ \frac{\partial \bar{\sigma}}{\partial \alpha} \right\} = - \left\{ \frac{\partial \bar{\sigma}}{\partial \sigma} \right\} \quad (43)$$

Substituting Eq. 43 into Eq. 42 and using Eq. 41 yields the desired expression for $d\mu$.

$$d\mu = \frac{\left[\frac{\partial \bar{\sigma}}{\partial \sigma} \right] \{d\sigma\}}{\left[\frac{\partial \bar{\sigma}}{\partial \sigma} \right] \{\sigma - \alpha\}} \quad (44)$$

Since the stress increment is known from an earlier calculation it is a simple matter to evaluate $d\mu$ through Eq. 44 and then $\{d\alpha\}$ through Eq. 41. Thus the computational procedure is complete.

Kinematic hardening requires seven arrays, three strains, three α 's, and the equivalent uniaxial strain for the determination of H' . This is two more arrays than needed for isotropic hardening. There is no appreciable additional computational effort required to use kinematic hardening.

Comparison of Isotropic and Kinematic Hardening*

Comparing the fundamental equations used for isotropic and kinematic hardening reveals several differences. For initial loading the expressions for $d\bar{\epsilon}^P$ given by Eqs. 33 and 40 are different. For isotropic hardening the denominator contains H' whereas for kinematic hardening the same term is $[\frac{\partial \bar{\sigma}}{\partial \sigma}] [H'] \{\frac{\partial \bar{\sigma}}{\partial \sigma}\}$. It should also be noted that $\bar{\sigma}$ is defined differently in isotropic and kinematic hardening.

Both isotropic and kinematic hardening have been coded and a comparison made of results. One such comparison for the center deflection of an impulsively loaded plate is shown in Fig. 2. It is observed in Fig. 2 that the results for the initial peak are almost identical for isotropic and kinematic hardening. However, the "snap-back" deflection is appreciably different with kinematic hardening showing that the plate returns to the original position. It should be observed that there is appreciable strain hardening in the results shown in Fig. 2. To explain this behavior consider the simple one dimensional structure shown in Fig. 3, which is loaded into the plastic range with appreciable strain hardening and then released. Isotropic hardening predicts a final deflection which is approximately equal to the deflection when the structure is released. However, due to the large amount of strain hardening, kinematic hardening predicts a plastic instability in the reverse direction. This is obviously a contradiction to experimental observation and could lead to misleading results. It should be noted in Fig. 3 that the value of H' is assumed to depend on

*Appreciation is expressed to Dr. Nicholas Perrone of the Office of Naval Research for his discussion on this subject.

the equivalent uniaxial plastic strain only. This could be easily changed for a one dimensional state of stress but to the authors' knowledge has not been developed for the plane stress case.

The net result of this comparison is that neither isotropic nor kinematic hardening represents the true situation when appreciable strain hardening occurs. However, it is felt that isotropic hardening will yield more realistic results for appreciable strain hardening and is used in the computer code.

SOLUTION PROCEDURE

Equation 20 is solved by the Houbolt solution procedure. The purpose of this section is to review the Houbolt procedure and to discuss the approximation of the loads vector.

In the Houbolt method the accelerations in Eq. 20 are replaced by a finite difference approximation of the second derivative. This substitution allows development of recursion relations which can be used for the step-by-step calculation of the displacements of the shell and stiffeners.

The accelerations of the nodes of the shell are approximated by the third order backwards difference expression

$$\{\ddot{q}_{n+1}\} = \frac{1}{(\Delta t)^2} \{2q_{n+1} - 5q_n + 4q_{n-1} - q_{n-2}\} \quad (45)$$

The accuracy of this representation is of the order $(\Delta t)^2$.

Substituting Eq. 45 into Eq. 20 and simplifying yields

$$(2[M] + (\Delta t)^2 [K])\{q_{n+1}\} = (\Delta t)^2 \{P_{n+1} + Q_{n+1}^*\} + [M]\{5q_n - 4q_{n-1} + q_{n-2}\} \quad (46)$$

This equation is valid for all time increments but must be modified for the first step since the values of $\{q_{-2}\}$ and $\{q_{-1}\}$ are not known. This occurrence is common when solving initial value problems by finite difference procedures and merely requires that a method be developed to start the solution. Equation 46 will, however, be used to calculate the displacements for all time increments except the first.

To start the solution, assume

$$\{\dot{q}_0\} = \frac{1}{6\Delta t} \{2q_1 + 3q_0 - 6q_{-1} + q_{-2}\} \quad (47)$$

and

$$\{\ddot{q}_0\} = \frac{1}{(\Delta t)^2} \{q_1 - 2q_0 + q_{-1}\} \quad (48)$$

The initial accelerations are obtained using Eq. 20 evaluated at $t = 0$ which gives

$$[M]\{\ddot{q}_0\} = \{P\} + \{Q^*\} - [K]\{q_0\} \quad (49)$$

Rearranging Eq. 48 gives

$$\{q_{-1}\} = (\Delta t)^2 \{\ddot{q}_0\} + \{2q_0 - q_1\} \quad (50)$$

By combining Eqs. 47 and 50 an expression for $\{q_{-2}\}$ is developed

$$\{q_{-2}\} = 6(\Delta t)^2 \{\ddot{q}_0\} + 6\Delta t \{\dot{q}_0\} + 9\{q_0\} - 8\{q_1\} \quad (51)$$

Substituting Eqs. 50 and 51 into Eq. 46 for the first time increment ($n = 0$) and approximating the forces at time, $t = 0$, provides an expression

in terms of the initial displacements, velocities, and accelerations which can be solved to obtain $\{q_1\}$

$$(6[M] + (\Delta t)^2 [K])\{q_1\} = (\Delta t)^2 \{P_{(0)} + Q^*(0,q)\} + [M]\{2(\Delta t)^2 \ddot{q}_0 + 6\Delta t \dot{q}_0 + 6q_0\} \quad (52)$$

This equation is used to determine the displacements at the end of the first time step. Using Eq. 50, a fictitious matrix of displacements, $\{q_{-1}\}$ can be determined. The displacements are then available so Eq. 46 can be used for each subsequent time step.

Examination of Eq. 46 shows that the applied and pseudo loads should be evaluated at time increment $n+1$ in the determination of the displacements at increment $n+1$. However $\{Q^*\}$ is a function of the displacements and thus Eq. 46 is basically a nonlinear set of algebraic equations. In the present research and as presented in Ref. 54 the problem is linearized by using an extrapolation procedure. Further, provisions are made for updating the pseudo force vector every m time increments to save on computer time. It has been found that if the pseudo loads vector is updated every time increment then a full linear extrapolation should be used. However, it has also been found that for some problems updating the pseudo loads vector, $\{Q^*\}$, every five time increments and using a half order extrapolation yields accurate results. For problems exhibiting a high degree of geometric nonlinearities it is advisable to update the pseudo loads vector every time increment to avoid numerical instabilities.

The option of updating the pseudo loads vector infrequently is quite valuable when using the Houbolt solution procedure. If high frequency

response is desired it is necessary to use a very small time increment due to inherent damping in the basic Houbolt procedure. However, this need not cost appreciably in computer run time provided the pseudo forces are not updated every time increment.

The loads vector $\{P\}$ is determined based on input loads at arbitrary times. For intermediate times the loads vector $\{P\}$ is determined by linear interpolation.

SHELL OF REVOLUTION

The previous sections have been devoted to structures or shells in general. The purpose of this section is to specialize the equations to the shell of revolution and present the fundamental theory used in this research.

For the linear stiffness matrix the shell of revolution is idealized as a sequence of curved elements. One such curved element is shown in Fig. 4. The curvature of the element is represented by a second order polynomial in the meridional distance s .

$$\phi = a_0 + a_1s + a_2s^2 \quad (53)$$

where s is the distance along the meridian of the element. The constants a_0 , a_1 , and a_2 are determined by requiring the actual shell and the idealized shell to have the same coordinates and slopes at the nodes. Detailed expressions for the a 's are given in Ref. 53.

Strain Displacement Relations

The strain displacement relations used in this research are based on the theory presented by Novozhilov.⁴⁵

$$\begin{aligned}
 \epsilon_s &= \hat{e}_s + z\hat{\kappa}_s + \frac{1}{2} \hat{e}_{13}^2 \\
 \epsilon_\theta &= \hat{e}_\theta + z\hat{\kappa}_\theta + \frac{1}{2} \hat{e}_{23}^2 \\
 \epsilon_{s\theta} &= \hat{e}_{s\theta} + z\hat{\kappa}_{s\theta} + \hat{e}_{13}\hat{e}_{23}
 \end{aligned} \tag{54}$$

where ϵ_s , ϵ_θ , and $\epsilon_{s\theta}$ are the total strains in the meridional and circumferential directions and the shear strain respectively. It should be noted that Eqs. 54 are valid for moderate rotations only. The expressions for the various terms in Eqs. 54 are given by:

$$\begin{aligned}
 \hat{e}_s &= (\partial u / \partial s) - \phi' w \\
 \hat{e}_\theta &= (1/r)[(\partial v / \partial \theta) + u \sin \phi + w \cos \phi] \\
 \hat{e}_{s\theta} &= (1/r)(\partial u / \partial \theta) - (v/r) \sin \phi + \partial v / \partial s
 \end{aligned} \tag{55}$$

$$\begin{aligned}
 \hat{e}_{13} &= (\partial w / \partial s) + u \phi' \\
 \hat{e}_{23} &= (1/r) (\partial w / \partial \theta) - (v \cos \phi) / r
 \end{aligned}$$

$$\begin{aligned}
 \hat{\chi}_s &= - \partial \hat{e}_{13} / \partial s \\
 \hat{\chi}_\theta &= - (1/r) (\partial \hat{e}_{23} / \partial \theta) - (1/r) \sin \phi \hat{e}_{13}
 \end{aligned} \tag{56}$$

$$\hat{\chi}_{s\theta} = - (1/r) (\partial \hat{e}_{13} / \partial \theta) + (\sin \phi / r) \hat{e}_{23} - \partial \hat{e}_{23} / \partial s$$

Linear Stiffness Matrix

The linear stiffness matrix is obtained based on orthotropic material and neglecting transverse shear deformations. The strain energy expression is given in Ref. 49. The displacement functions used in obtaining the linear stiffness matrix are given by:

$$\begin{aligned}
 w &= (\alpha_1^i + \alpha_2^i s + \alpha_3^i s^2 + \alpha_4^i s^3) \cos i\theta \\
 u &= (\alpha_5^i + \alpha_6^i s + \beta_1^i s (s-L) + \beta_2^i s^2 (s-L)) \cos i\theta \\
 v &= (\alpha_7^i + \alpha_8^i s + \beta_3^i s (s-L) + \beta_4^i s^2 (s-L)) \sin i\theta
 \end{aligned} \tag{57}$$

Note that the summation convention is being used. L is the meridional length of the element. It should be noted that only the terms due to symmetric loads about $\theta = 0$ are included. The terms β_1 , β_2 , β_3 , and β_4 , are eliminated by static condensation in the Fourier terms $i = 0$ and 1 only. These are the only terms in the Fourier expansion which contribute to rigid body motion and these terms are needed for that purpose. Static condensation is not used for the higher Fourier terms as experience has shown that a "too flexible" stiffness matrix may be obtained.

After the assumed displacement functions and strain displacement relations are substituted into the strain energy expression, the element stiffness matrix for each Fourier term is determined by numerical integration. Twenty-nine Simpson stations are used to integrate along the meridian of the shell element.

Mass Matrix

A consistent mass matrix based on linear displacement functions in u and v and a cubic displacement function in w is used in this research. Rotary inertia is included but has not been found to be significant for problems considered to date.

Nonlinear Terms

In contrast to the highly accurate procedure used in evaluating the linear stiffness matrix, an extremely simplified procedure is used in evaluating the effects of both material and geometric nonlinearities. This consists of using conical frustum elements and finite difference expressions for the strains, rotations, changes in curvature, and twist and evaluating the integrals over the length by strip integration. This section presents the details of this procedure.

Referring to the expressions for the strains, rotations, curvatures, and twist given by Eqs. 55 and 56 and using the fact that the displacements are represented as Fourier series in the circumferential angle θ the various terms may be written as:

$$\begin{aligned}
 \hat{e}_s &= e_s^i \cos i\theta & \hat{e}_\theta &= e_\theta^i \cos i\theta \\
 \hat{e}_{s\theta} &= e_{s\theta}^i \sin i\theta & \hat{e}_{13} &= e_{13}^i \cos i\theta \\
 \hat{e}_{23} &= e_{23}^i \sin i\theta & \hat{\kappa}_s &= \kappa_s^i \cos i\theta \\
 \hat{\kappa}_\theta &= \kappa_\theta^i \cos i\theta & \hat{\kappa}_{s\theta} &= \kappa_{s\theta}^i \sin i\theta
 \end{aligned} \tag{58}$$

where e_s^i , e_θ^i , $e_{s\theta}^i$, e_{13}^i , e_{23}^i , κ_s^i , κ_θ^i , and $\kappa_{s\theta}^i$ may at most depend only on the meridional distance, s , along the element. However, using finite difference expressions for these terms their values may be computed at the middle of the element and held constant over the meridional length.

The use of finite difference expressions permits the individual Fourier components to be written as:

$$\begin{aligned}
 e_s^i &= \frac{\partial e_s^i}{\partial q_j} q_j & e_\theta^i &= \frac{\partial e_\theta^i}{\partial q_j} q_j \\
 e_{s\theta}^i &= \frac{\partial e_{s\theta}^i}{\partial q_j} q_j & e_{13}^i &= \frac{\partial e_{13}^i}{\partial q_j} q_j \\
 e_{23}^i &= \frac{\partial e_{23}^i}{\partial q_j} q_j & \kappa_s^i &= \frac{\partial \kappa_s^i}{\partial q_j} q_j \\
 \kappa_\theta^i &= \frac{\partial \kappa_\theta^i}{\partial q_j} q_j & \kappa_{s\theta}^i &= \frac{\partial \kappa_{s\theta}^i}{\partial q_j} q_j
 \end{aligned} \tag{59}$$

There is no summation on i , which indicates the particular term in the Fourier expansion. The detailed expressions for the partial derivatives are given in Appendix A. The partial derivatives in Eq. 59 are independent of s , θ , and the displacements, but may depend on the Fourier number.

Specializing Eq. 23 to the shell of revolution yields:

$$Q_j^{Ii} = \iiint \left[\frac{\partial \epsilon}{\partial q_j} \right] [D] \{ \epsilon^P + \epsilon^T + \dots \} r d\theta ds dz \tag{60}$$

where i and j are the Fourier number and degree of freedom respectively.

All terms are assumed to be constant over s , then

$$\int ds = L \quad (61)$$

Further, the expression is simplified with the following definition

$$\{C\} = [D]\{\epsilon^P + \epsilon^T + \dots\} rL \quad (62)$$

where r = radial distance to the middle of the element.

Using Eqs. 54, 58, and 59 the expression for the pseudo force may be written as

$$\begin{aligned} Q_j^{Ii} = & \iint \left[\frac{\partial e_s^i}{\partial q_j^i} \cos i\theta + \hat{e}_{13} \frac{\partial e_{13}^i}{\partial q_j^i} \cos i\theta + z \frac{\partial \kappa_s^i}{\partial q_j^i} \cos i\theta \right) C_1 \\ & + \frac{\partial e_\theta^i}{\partial q_j^i} \cos i\theta + \hat{e}_{23} \frac{\partial e_{23}^i}{\partial q_j^i} \sin i\theta + z \frac{\partial \kappa_\theta^i}{\partial q_j^i} \cos i\theta \right) C_2 \\ & + \left(\frac{\partial e_{s\theta}^i}{\partial q_j^i} \sin i\theta + \hat{e}_{13} \frac{\partial e_{23}^i}{\partial q_j^i} \sin i\theta + \hat{e}_{23} \frac{\partial e_{13}^i}{\partial q_j^i} \cos i\theta \right. \\ & \left. + z \frac{\partial \kappa_{s\theta}^i}{\partial q_j^i} \sin i\theta \right) C_3 \right] dz d\theta \end{aligned} \quad (63)$$

where there is no summation on i . C_1 , C_2 , and C_3 are the three components of $\{C\}$ given by Eq. 62.

Applying the same logic to Eq. 26 the pseudo forces due to geometric nonlinearities for the shell may be written as:

$$\begin{aligned}
 Q_i^{NLi} = & - \int \left[\frac{\partial e_s^i}{\partial q_j^i} \cos i\theta \bar{C}_1 + \frac{\partial e_\theta^i}{\partial q_j^i} \cos i\theta \bar{C}_2 + \frac{\partial e_{s\theta}^i}{\partial q_j^i} \sin i\theta \bar{C}_3 \right] d\theta \\
 & - \int \left[\hat{e}_{13} \frac{\partial e_{13}^i}{\partial q_j^i} \cos i\theta \bar{C}_1 + \hat{e}_{23} \frac{\partial e_{23}^i}{\partial q_j^i} \sin i\theta \bar{C}_2 \right. \\
 & \left. + (\hat{e}_{13} \frac{\partial e_{23}^i}{\partial q_j^i} \sin i\theta + \hat{e}_{23} \frac{\partial e_{13}^i}{\partial q_j^i} \cos i\theta) \bar{C}_3 \right] d\theta
 \end{aligned} \tag{64}$$

where there is no summation on i and

$$\{\bar{C}\} = (t)(r)(L) [D] \{\epsilon_{NL}\} \tag{65}$$

$$\{\bar{C}\} = (t)(r)(L) [D] \{\hat{e} + \epsilon_{NL}\} \tag{66}$$

Equations 63 and 64 are the basic equations needed to compute the pseudo forces due to material and geometric nonlinearities. The C 's depend on z and θ in Eq. 63 and \bar{C} and $\bar{\bar{C}}$ depend on θ in Eq. 64. The integral through the thickness is performed by Simpson's rule in Eq. 63 and it has been found that 5 to 7 Simpson stations are quite adequate. The integrations around the circumference in Eqs. 63 and 64 are performed using a modified Simpson's rule, the modification being that the second order function of θ is weighted with $\sin i\theta$ and/or $\cos i\theta$ to obtain the integrals. Before

this modified Simpson's rule was incorporated it was found that the number of stations around the circumference was dictated by the number needed to integrate $\cos i\theta$ or $\sin i\theta$ and could be quite large.

RING STIFFENERS

The ring stiffeners for any element may be constructed of as many as three different segments and may vary from element to element. This permits an exact representation of stiffeners in the form of T or I sections. However a Z section may be represented only approximately as the product of inertia terms are neglected.

The mass, stiffness, and strain hardening for the stiffeners may be different from those of the adjoining shell. The effects of eccentricity are accounted for in all calculations where the reference surface is taken to be the mid-surface of the shell. The ring stiffeners are assumed to be in a state of uniaxial stress in the circumferential direction. Under this assumption strain energy per element based on linear theory is given by

$$U_R^L = \frac{EN}{2} \int [\hat{\epsilon}_\theta^2 + z \hat{e}_\theta \hat{\kappa}_\theta + z^2 \hat{\kappa}_\theta^2] r d\theta dz ds \quad (67)$$

where N is the number of stiffeners per element. Integrating Eq. 67 through the thickness yields

$$U_R^L = \frac{(E)(N)(t)}{2} \int [\bar{e}_\theta^2 + \bar{z} e_\theta \kappa_\theta + I \kappa_\theta^2] r d\theta ds \quad (68)$$

where \bar{z} is the distance from the mid-surface of the shell to the centroid of the stiffeners and I is the area moment of inertia about the mid-surface

of the shell.

The terms of the stiffness matrix are obtained from Eq. 68 by taking the second derivative with respect to the generalized degrees of freedom.

$$K_{ij}^R = \frac{\partial^2 U_L^R}{\partial q_i \partial q_j} \quad (69)$$

In the numerical computation of the contribution of the stiffeners to the element stiffness matrix the N stiffeners are assumed to be "smeared" over the meridional length of the element. Integration is performed along the length using Simpson's rule.

For most practical applications the ring stiffeners are discrete and "smearing" can lead to appreciable error. This error is avoided by using a very short element for the discrete stiffeners, thus avoiding any "smearing" error.

The pseudo forces due to initial (plastic) strains are given by Eq. 63 with only C_2 being non zero. Thus the pseudo force expression becomes:

$$Q_j^{Ii} = N \iint \left[\left(\frac{\partial e_i}{\partial q_j} \cos i\theta + z \frac{\partial \kappa_\theta^i}{\partial q_j} \cos i\theta \right) E (\epsilon^P + \epsilon^T + \dots) rL \right] dz d\theta \quad (70)$$

Equation 70 is evaluated using either strip or Simpson integration over each segment of the stiffener and a modified Simpson integration around the circumference. Note that strip integration has been used over the meridional length.

The pseudo forces due to geometric nonlinearities are given by Eq. 26 which when specialized to the ring becomes:

$$\begin{aligned}
Q_j^{NLi} = & - (E)(t)(r)(L)(N) \int \left[\left(\frac{\partial e_\theta^i}{\partial q_j} \cos i\theta + \bar{z} \frac{\partial \kappa_\theta^i}{\partial q_j} \cos i\theta \right) \frac{1}{2} \hat{e}_{23}^2 \right] d\theta \\
& - \int \hat{e}_{23} \frac{\partial e_{23}^i}{\partial q_j} \sin i\theta \left(e_\theta + \frac{1}{2} \hat{e}_{23}^2 + \bar{z} \hat{\kappa}_\theta \right) d\theta
\end{aligned} \tag{71}$$

where \bar{z} is the distance from the mid-surface of the shell to the centroid of the complete ring stiffener. There is no summation on i in either Eqs. 70 or 71.

SPRING SUPPORTS

There are frequently shells of revolution which have intersecting supports at various locations around the circumference. The missile tubes and platforms in submarines serve as specific examples of such supports. In the present research these supports are included as linear elastic springs and are incorporated into the basic equations as pseudo forces on the right hand side of the equations of equilibrium. This procedure is rather straightforward but can lead to numerical instability problems for overly stiff supports. Further the supports must be included so as not to prevent rigid body translation of the complete system. To accomplish this latter objective the supports are treated as coupled linear elastic springs.

The general equations for the forces and moments due to the spring supports are given by:

$$\begin{aligned}
\{F_s\} &= [K_F] \{q\} \\
3 \times 1 & \quad 3 \times 3 \quad 3 \times 1
\end{aligned} \tag{72}$$

and

$$\{M\} = [K_M] \begin{Bmatrix} e_{13} \\ e_{23} \end{Bmatrix} \quad (73)$$

where \bar{q} are the deflections at the center of the element in cylindrical coordinates. \bar{q}_1 , \bar{q}_2 , and \bar{q}_3 are the axial circumferential and radial displacements respectively. e_{13} and e_{23} are rotations about the circumferential and meridional directions respectively.

As a simple example consider a single support on a circumferential ring as shown in Fig. 5. The support as shown acts in the q'_1 direction only and the forces are given by:

$$\begin{Bmatrix} F'_1 \\ F'_2 \\ F'_3 \end{Bmatrix} = \begin{bmatrix} K & 0 & 0 \\ 0 & 0 & 0 \\ 0 & 0 & 0 \end{bmatrix} \begin{Bmatrix} q'_1 \\ q'_2 \\ q'_3 \end{Bmatrix} \quad (74)$$

where q'_2 and q'_3 are in the other two orthogonal directions.

Next the q 's are related to the \bar{q} 's through the transformation

$$\begin{Bmatrix} q'_1 \\ q'_2 \\ q'_3 \end{Bmatrix} = \begin{bmatrix} 0 & \cos\theta_s & \sin\theta_s \\ 0 & 0 & 0 \\ 0 & 0 & 0 \end{bmatrix} \begin{Bmatrix} \bar{q}_1 \\ \bar{q}_2 \\ \bar{q}_3 \end{Bmatrix} \quad (75)$$

Using Eq. 75 to transform the displacements and forces F' , the matrix $[K_F]$ becomes

$$[K_F] = \begin{bmatrix} 0 & 0 & 0 \\ \cos\theta_s & 0 & 0 \\ \sin\theta_s & 0 & 0 \end{bmatrix} \begin{bmatrix} K & 0 & 0 \\ 0 & 0 & 0 \\ 0 & 0 & 0 \end{bmatrix} \begin{bmatrix} 0 & \cos\theta_s & \sin\theta_s \\ 0 & 0 & 0 \\ 0 & 0 & 0 \end{bmatrix} \quad (76)$$

Carrying out the indicated matrix multiplication in Eq. 76 yields:

$$[K_F] = K \begin{bmatrix} 0 & 0 & 0 \\ 0 & \cos^2\theta_s & \cos\theta_s \sin\theta_s \\ 0 & \cos\theta_s \sin\theta_s & \sin^2\theta_s \end{bmatrix} \quad (77)$$

The matrix of coefficients given by Eq. 77 restricts motion in the q_i direction but permits the entire system to translate in the horizontal direction. It should be noted that this objective could not be accomplished without permitting a complete matrix of spring constants.

An interesting application of the spring support idea is to represent an incomplete clamped circular ring or cylindrical panel. The spring constants in these cases should be very large - - ideally infinity. However in practice these spring constants may be selected by assuming that the supports are short stubby beams as compared with the actual structure. It has been found that the spring constants may be made quite large without introducing numerical stability problems. Specific examples are given in the section on application.

COMPUTATIONAL PROCEDURE

The purpose of this section is to present, in some detail, the computational procedure used to compute the pseudo forces due to geometric and material nonlinearities. This should not be interpreted to imply that the other portions of the numerical process are unimportant. However, the details of much of the procedure for computing mass and stiffness matrices are the same as were presented in earlier works.^{49,53}

In an earlier computer code called DYNASOR for the geometric nonlinear analysis of shells of revolution the integrals around the circumference were evaluated exactly. To perform this task several three and four dimensional arrays were needed where each dimension was the number of Fourier terms used in the expansion. Further, these arrays were used in three and four nested DO loops within the program. The net result of the formulation used in DYNASOR was that storage requirements and computer run times restricted the number of Fourier terms that could be used.

During the course of the present research, it was found that numerical integration around the circumference is a very efficient computational procedure both from the viewpoint of computer time required and storage allocations. The importance of the modified Simpson's rule cannot be overemphasized. The present code called DYNAPLAS is considerably more efficient especially when a large number of Fourier terms is being used. Considering the fact that DYNASOR required shorter computer run times than comparable computer codes, the present code, DYNAPLAS, should be capable

of solving large scale problems in realistic computer run times.

The pseudo forces are computed in one rather long (1400 statement) subroutine called QPRIME. The long length is due to the large number of statements inside a DO loop over the number of modified Simpson stations around the circumference. This also explains why a reduction in the number of stations around the circumference through the use of a modified Simpson's integration saves appreciably on computer run times.

The key to an efficient computational procedure is the computation of the partial derivatives given in Eq. 59 and tabulated in Appendix A. While the term partial derivatives is used here they could equally well be called coefficients or any similar terminology as they do not depend on the displacements. At times the term partial derivatives leads one to believe that the Eqs. 59 are only approximate whereas they are exact regardless of the magnitude of the generalized displacements. The second step in the computational procedure is to compute linear strains, rotations, changes in curvature, and twist for each Fourier term as given by Eq. 59. With these preliminary calculations out of the way a DO loop over the number of integration stations around the circumference is entered. For each modified Simpson station the following calculations are performed.

- A. Compute the strains, rotations, curvature, and twist in accordance with Eq. 58.
- B. If stations have not yielded before, check for yielding. This calculation involves calculating the stress in accordance with Eqs. 9 and 10 and the evaluation of $\bar{\sigma}$ from Eq. 27.
- C. For each Simpson station through the thickness compute the increment

of plastic strain. This involves Eqs. 28, 30, 31, and 33. Further, this section involves some rather complex logic to transverse the region from elastic to elastic-plastic behavior and checks for unloading and reloading.

- D. Compute the pseudo forces due to initial strains using Eq. 63.
- E. Compute the pseudo forces due to geometric nonlinearities using Eq. 64.

COMPUTER PROGRAMS

The computational algorithm presented here has been coded into two FORTRAN programs called SAMMSOR III and DYNAPLAS. These two codes are essentially an extension of two SOR codes, SAMMSOR II and DYNASOR II, which have been operational since 1970. The extensions include elastic-plastic material behavior, ring stiffeners, and the effects of other internal and/or external stiffening members in addition to the large deflection capability of DYNASOR II.

As in the SOR series of codes the dynamic analysis is conducted by first executing the SAMMSOR III code to obtain an output tape containing the stiffness and mass matrices for the particular geometry being studied. DYNAPLAS is then executed to solve the dynamic equations for a specific set of initial conditions, boundary conditions and loading history. A subsequent analysis of the same problem with, for example, a different loading history requires only the execution of DYNAPLAS.

The SAMMSOR III code utilizes a highly refined curved shell of revolution element in addition to beam type ring stiffeners. The shell element utilizes cubic displacement functions for the normal and in-plane displacements and, through static condensation, a basic eight degree of freedom stiffness matrix is generated. A mesh generating routine is included which allows the user to input the geometry of complicated shells of revolution with only a minimum of input information. The ring stiffeners are assumed to have zero products of inertia

but may be eccentrically located and may be formed by as many as three rectangular flange members.

In addition to the stiffness and mass matrices generated by SAMMSOR III, DYNAPLAS requires the uniaxial stress-strain data for the shell and stiffeners, the boundary conditions, the initial displacement and velocity conditions, and the applied load as a function of time. In addition, a number of other control constants are required; for example the specific Fourier terms to be utilized in the analysis, the time increment, the number of integration stations to be utilized in numerically integrating over the volume, print parameters, etc. The applied load history may be described by specifying either a pressure distribution over the element or the Fourier coefficients of the distribution at discrete time intervals with a linear variation being assumed between the specified times. For a particular element, the pressure distribution is assumed to be constant in the meridional direction and vary as a step function in the circumferential direction. In addition, the code is capable of accepting concentrated ring loads at each node. The uniaxial stress-strain data is described by inputting a piecewise linear curve with as many as five stress-strain data points. The material characteristics may vary from element to element. The code may of course be run with plasticity and/or geometric nonlinear effects omitted.

The computer code has a restart provision permitting the program to be restarted at a particular time increment once the program has been

run up to that time. Restart information is placed on tape periodically during the execution of DYNAPLAS. If subsequent analysis of the output by the user indicates that, for example, a smaller time increment is needed or the nonlinear forces need to be updated more often, the program can be automatically cycled to any time increment for which restart information is stored on tape and then the analysis restarted with new input parameters (smaller time increment, etc).

The program output consists of all input control words, input loads, generalized forces, stiffness and mass matrices, and the resultant displacements, stresses and strains through the thickness and around the circumference. Various print parameters allow the user to select as much or as little of the above output as he desires.

In order to make the program more flexible variable or dynamic dimensioning has been used on forty-four main arrays in DYNAPLAS. A blank common block is dimensioned for a certain number of storage locations in the main program and is used as a dynamic storage area. The forty-four arrays are then implicitly equivalenced to various portions of the blank common by the subroutine call list. These variables are variable dimensioned in all subroutines for the number of elements, harmonics, etc. A subroutine is called from the main program which scans the input files to determine the necessary storage requirements based on the number of elements, harmonics, etc. If the required number of storage locations is less than what the blank common is dimensioned, then execution of the data set begins. This subroutine also determines (based

on the input data) the beginning point of each of the forty-four arrays relative to the first location of the blank common. This feature allows the user to set the size of the blank common based on (a) available core size and (b) program size required to solve a problem. The values of the various input parameters (such as number of elements, Fourier terms, integration stations, etc.) may be input in any combination as long as the dynamic storage area is not exceeded.

These programs have been written in standard FORTRAN IV language. The programs are operational on the IBM 360/65 computer at Texas A&M University and the CDC 6600 computer at Sandia Laboratories. As usual, the IBM version of the programs requires double precision arithmetic in critical areas. Utilizing mixed mode arithmetic, SAMMSOR III requires approximately 180,000 bytes of storage (fifty elements). DYNAPLAS requires approximately 160,000 bytes of storage plus the dynamic storage area. A fifty element idealization utilizing ten Fourier terms requires approximately 200,000 bytes of dynamic storage area (IBM 360/65).

Considering the complexity of the computer program it is highly efficient. For example the solution to the ring presented in Figure 2 required less than 20 seconds of IBM 360/65 computer time. The analysis of the circular plate presented in Figure 9 required about 3 minutes of IBM 360/65 time. The solution to the asymmetrically loaded truncated cone shown in Figure 11 using thirty elements and ten Fourier terms required 30 minutes of CDC 6600 computer time (updating the nonlinear forces at each time increment). If the nonlinear forces are updated

every three time increments, the solution may be obtained in only 10 minutes of CDC 6600 computer time.

The SAMMSOR III code has been operational for several years and its validity demonstrated on many test cases. The DYNAPLAS code has been in operation for about one year at Texas A&M University and Sandia Laboratories. Based on the test cases reported herein, good agreement has been noted between DYNAPLAS and numerical results obtained using other computer codes. Considering the assumptions in the plasticity theory, reasonable agreement has been achieved between DYNAPLAS and experimental results.

Copies of the users manuals* and computer code are available to qualified users upon request. Requests should be addressed to Dr. Walter E. Haisler, Aerospace Engineering Dept., Texas A&M University, College Station, Texas 77843.

-
- *1. Haisler, W.E., Stricklin, J.A., and Von Rieseemann, W.A., "DYNAPLAS - A Finite Element Program for the Dynamic, Elastic-Plastic, Large Deflection Analysis of Stiffened Shells of Revolution," SLA-73-0127, Sandia Laboratories, Albuquerque, New Mexico (Also Rpt. 72-27, Aerospace Engineering Department, Texas A&M University), January 1973.
 2. Haisler, W.E., Stricklin, J.A., and Von Rieseemann, W.A., "SAMMSOR III - A Finite Element Program to Determine Stiffness and Mass Matrices of Ring-Stiffened Shells of Revolution", SLA-73-0126, Sandia Laboratories, Albuquerque, New Mexico (Also Rpt. 72-26, Aerospace Engineering Department, Texas A&M University, College Station, Texas), January 1973.

Check Out Problems

The purpose of this section is to present the solutions to a substantial number of problems. The problems vary from a simple symmetrically deformed ring to the response of a hypothetical but complex submarine. The solutions show the versatility of DYNAPLAS as well as its limitations.

Static Solution for Spherical Cap

A doubly curved shell element is used in the computation of the linear stiffness matrix, but, conical frustum elements are used in the calculation of the effects due to nonlinearities including the stress resultants. As past experience⁵³ has shown that the use of only conical frustum elements gives a residual bending moment, it was deemed necessary to check the accuracy of using conical frustum elements for the computation of the stress resultants.

The problem chosen to check the accuracy of the computation of the stress resultants was the static solution for a linearly elastic spherical cap under an internal pressure as shown in Fig. 6. The cap has a radius of 100", a thickness of .5", a Young's modulus of 10×10^6 psi, and a Poisson's ratio of 0.2. The static solution was obtained by using a large time increment in the solution procedure. The large time increment introduces a considerable amount of artificial damping in the basic Houbolt solution procedure and thus yields a static solution after a relatively few time steps. This same procedure is used on

the submarine problem, presented later, to obtain the solution under a hydrostatic pressure before the transient load is applied.

The results shown in Fig. 6 are for 10 and 30 equally spaced elements in DYNAPLAS and the converged solution. It is noted that the 30 element idealization is in excellent agreement with the converged solution. Further there is no residual bending moment for either the coarse or fine element breakdown. The conclusion drawn from this study is that the stress resultants may be accurately computed based on conical frustum elements.

Finally it should be explained why conical frustum elements are used for nonlinear terms. The answer is simply that the use of finite difference expressions to compute the strains using curved elements shows straining under rigid body motion.

Symmetrically Impulsively Loaded Ring

The first example of an elastic-plastic dynamic response is a plane strain ring subjected to a symmetrical impulse loading giving an initial velocity of 4911.7 in/sec. The ring had a 10" radius, a thickness of .1", and a density of .1 lb/in.³ The yield stress was taken to be 42,400 psi and the problem was studied for various amounts of strain hardening. The results for the radial deflection vs. time are shown in Fig. 7 along with results given by Duffey and Krieg¹⁴ and computer results obtained from the computer code UNIVALVE.³² Results are presented for three different values of the strain hardening parameter, $\lambda = E_T/E$. It is noted that all three solutions

are in excellent agreement. A problem similar to this one was solved where the impulsive load was applied as a high intensity pressure over a short duration of time. The results were found to agree with those obtained using an initial velocity based on same impulse.

Free Ring Under Half-Cosine Impulsive Load

The first example solution for asymmetrical loading is a free-free plane strain ring under a half-cosine impulsive loading. The aluminum ring had a radius of 11", a thickness of .15", and a density of .09997 lb/in³. The stress-strain curve was assumed to have a yield stress of 30,000 psi, a secondary modulus of 5×10^6 psi to a total strain of .009 in/in, and perfectly plastic thereafter. The solution through DYNAPLAS was obtained using 5 Fourier terms and a time increment of 0.5 μ sec. The results for the deflection at $\theta=0$ vs. time are presented in Fig. 8 along with results from the computer codes SPECTRE⁸ and UNIVALVE.³² Results from DYNAPLAS are given for updating the pseudo forces every time increment in conjunction with an extrapolation factor of 1.0 and updating every 5 time increments with an extrapolation factor of .5. It is noted that the two solutions agree quite well with each other as well as with the results from SPECTRE and UNIVALVE.

This problem was used to check various provisions in the computer code. The problem was solved as a ring, a shell (with slight modification to computer code) and as three flanges, two of which were eccentrically located. The problem was also solved as a ring with

the reference surface at the inner edge of the ring. The solutions for all these cases agreed quite well with each other.

Figure 9 presents the plastic strain at the outer surface and $\theta = 0$ vs. time for 3, 5, and 9 modified Simpson's stations around the circumference. It is noted that reasonably good results are obtained with only 3 modified Simpson's stations. The deflections agreed quite well with the results presented in Fig. 8 for all three cases.

Clamped Ring Under Impulsive Loading

Wu and Witmer^{62,63} have conducted extensive studies of the highly nonlinear dynamic response of rings and reported experimental results based on earlier tests. One of the rings which they studied is shown in Fig. 10. The ring had a radius of 2.935 in., a thickness of .123 in, and a density of $.25 \times 10^{-3}$ lb-sec²/in⁴. The yield stress was 42,800 psi and the secondary modulus was 78,700 psi. The ring subtended an angle of 315° and the boundaries were clamped. An impulse giving an initial velocity of 4862 in/sec was applied over a 120° segment.

The theoretical solution by DYNAPLAS was obtained using 5, 10, and 15 Fourier terms. Time increments used were 5 μ sec for the 5 and 10 term analysis and 2 μ sec for the 15 term analysis. It should be noted that the deflections are very large with the outer edge of the ring almost reaching the origin of the original circle. The 15 Fourier term solution shows excellent agreement with the experimental

results.

The clamped boundary condition was obtained by including springs at the supports. In an earlier run, one of the spring constants was arbitrarily set equal to 15×10^6 lb/in. It was found that this very large spring constant introduced a "flip-flop" response in the solution near the support. The portion of the ring very near the spring would be loading plastically in one direction at one time increment and be loading plastically in the opposite direction at the very next time increment. As this provision is unrealistic and not accounted for in DYNAPLAS, the stress deviated from the assumed stress-strain curve. However, the solution procedure did not diverge. To avoid this difficulty a physically reasonable support system was assumed to be represented by the bending of a strip with the same cross-section as the ring but only .5" long. This led to spring constants of 50,000 lb/in for the deflection springs and 25,000 in-lb/rad. for the rotational spring. The deflections and rotations at the boundary were so small as to be insignificant for all computer runs using these spring constants. The important point to be noted is that physically realistic spring constants must be used.

The case for 10 Fourier terms was first studied using 11 modified Simpson stations to integrate around the circumference. This led to a monotonically divergent solution at approximately 1000 μ sec. The problem was corrected by increasing the number of modified Simpson stations to 17. This is the only problem where this type of difficulty occurred but as a result it was concluded that a "safe"

number of Fourier stations is approximately twice the highest Fourier number being used. Undoubtly most problems may be solved using considerably fewer stations and thus saving appreciably on computer run times.

In the solution using 15 Fourier terms, 27 modified Simpson stations around the circumference and 7 Simpson stations were used through the thickness. The pseudo forces were updated every time increment resulting in a computer run time of 8 minutes (CDC 6600).

The results from DYNAPLAS for the total strain at the line of symmetry and on the outer surface are given in Fig. 11.

It is noted that the maximum strain reaches a value of 8.5%. The angle of rotation as a function of the angle around the circumference at 1000 μ sec is shown in Fig. 12. It is noted that the maximum rotation is .6 radians at 1000 μ sec and probably approaches 1 radian at 2000 μ sec. The rotations were obtained from the solution using 10 Fourier terms.

Cylindrical Shell Under Impulsive Load

The final deflection of a clamped cylindrical shell under a half-cosine impulsive loading is given in Fig. 13. The length of the cylinder was 6 inches and was idealized using 10 finite elements along half the length and 5 Fourier terms. The final deflection was obtained by running DYNAPLAS with a small time increment until all elements began unloading. The time increment was then increased and the solution restarted. This large time increment damped out the

motion quite rapidly. Shown in Fig. 13 are results from DYNAPLAS, SHORE,⁵⁷ and experimental results.³⁵ Reasonable agreement among the results is noted but it should be pointed out that the final deflection shape is not a good measurement of the accuracy of a computer code.

Circular Plate Under Impulsive Load

The next problem is the analysis of a circular plate shown in Fig. 14 and 15. The experimental results were taken from Ref. 15. In the experimental procedure the plate was supported by two massive rings 2" in thickness and connected with 12 1/2 inch bolts at a radius of 4 inches. The edge of the rings was 3" from the center. It was observed after the experiment that some slippage did occur at the inner edge of the ring. To represent the boundary conditions in the theoretical analysis it was assumed that the circular plate was clamped at the bolt circle and on rollers for the portion inside the bolt circle covered by the ring. These boundary conditions are duplicated in the sketch in Figs. 14 and 15.

In the analysis using DYNAPLAS eleven finite elements were used. Nine were equally spaced over the inner portion of the ring and two elements were used to represent the portion of the ring under the rollers. A time increment of 1 μ sec was used in DYNAPLAS. The stress-strain curve was represented by an initial elastic modulus of 10^7 psi to a strain of .00424 in/in, then a secondary modulus of 3.29×10^6 psi to a total strain of .00449 in/in, and perfectly

plastic behavior thereafter.

Experimental and theoretical results for the deflection at the center of the plate are shown in Fig. 14. It is observed that there is good agreement through the initial peak deflection and over part of the unloading curve. However the experimental results deviate from theoretical results at later time increments.

The experimental and theoretical values for the meridional strain on the top of the plate at a distance of 2.125 inches from the center are shown in Fig. 15. Considering the closeness of this point to the edge of the supporting ring the agreement between theory and experiment is considered to be acceptable. Further if the strains were plotted to a scale necessary to represent the strain at the center of the plate very little difference in the experimental and theoretical points would be observed.

Truncated Cone Under Half-Cosine Impulse

The next problem studied was the large deflection elastic-plastic dynamic response of a truncated cone under a half cosine impulsively applied pressure. The truncated cone had a upper radius of 7.95", a lower radius of 10.23", a thickness of .5430" and a density of 1.88×10^{-4} lb sec²/in⁴. Additional details are given on Figs. 16, 17, and 18. The material was assumed to have a yield stress of 30,000 psi and to be elastic-perfectly plastic.

Results are presented for the deflections (Fig. 16) and strains (Figs. 17 and 18) as obtained from DYNAPLAS, REPSIL,^{24,52} and SHORE.⁵⁷

Considering the fact that the three computer codes are completely independent the agreement of displacements and strains presented in Figs. 16, 17, and 18 is considered to be outstanding and serves as a check on the accuracy of all three codes. However, based on the shown displacements, it is clear that the degree of geometric non-linearity is not severe.

In DYNAPLAS, the conical frustum shell was idealized as 30 equally spaced finite elements and 10 Fourier terms were used. Seven Simpson stations were used through the thickness and a 2 μ sec time step was used. Two runs were made varying the frequency of updating the pseudo forces and the number of modified Simpson stations around the circumference. Results were the same for both cases. In the first 13 Simpson stations were used and the pseudo forces were updated every three time increments with an extrapolation factor of 1.0. The computer run time was 10 minutes on the CDC 6600. In the second run 17 Simpson stations were used and the pseudo forces were updated every time increment. The computer run time was 30 minutes on the CDC 6600. Storage requirements were 88,000 words for the second case.

The SHORE code was run using 30 and 18 equally spaced increments along the meridian and around the circumference respectively. The computer run time was 22-1/2 minutes on the UNIVAC 1108 which is comparable to the case one run for DYNAPLAS.

Cylinder Under Moving Pressure Load

To illustrate the capabilities of DYNAPLAS to treat a complex moving pressure load, a clamped cylinder previously solved through REPSIL was chosen. The shell had a length of 5.958", a diameter of 5.958", a thickness of .042", and a density of .1 lb/in³. Young's modulus and Poisson's ratio were 10.5×10^6 psi and .3 respectively. The yield stress was chosen to be 44,000 psi and the material was taken to be elastic-perfectly plastic.

The pressure loading is given by

$$p(r\theta, t) = \begin{cases} 0 & \text{for } t < \frac{r\theta}{U} \\ \frac{P_0}{T} \left(\frac{r\theta}{U} + T - t \right) \cos \frac{2r\theta}{D} & \text{for } \begin{cases} \frac{r\theta}{U} \leq t \leq \frac{r\theta}{U} + T \\ -\frac{\pi D}{4} \leq r\theta \leq \frac{\pi D}{4} \end{cases} \\ 0 & \text{for } t > \frac{r\theta}{U} + T \\ 0 & \text{for } \frac{\pi D}{4} < |r\theta| < \frac{\pi D}{2} \end{cases}$$

where

D = diameter = 5.958"

U = velocity of pressure front = 24,800 in/sec.

T = duration of triangular pulse = 8.28743×10^{-6} sec.

P_0 = peak pressure at crown line = 28,000 psi.

The wave front velocity requires 200 μ sec to travel to $\theta = \pi/2$. The short duration of the pressure pulse yields a very high intensity pressure

extending over a very small angle of the shell.

In DYNAPLAS the shell was idealized as 10 equally spaced elements over 1/2 of the meridional length. The Fourier coefficients for the pressure loading were input every 4 μ sec with the computer code using linear interpolation at intermediate times. A time increment of 1 μ sec was used with the pseudo forces being updated every time increment.

The first run was conducted using 5 Simpson stations through the thickness and revealed a shortcoming of the DYNAPLAS computer code. The rotations at the nodes diverged with the value at one node increasing in the positive direction and the adjacent node diverging in the negative direction. After considerable deliberation it was concluded that the difficulty was caused by the extreme thinness of the shell (.042"). The elastic stiffness matrix simply has no resistance to rapid changes in angles. It was decided that for extremely thin shells it should be permissible to use effectively membrane theory to evaluate the effects of nonlinearities. This consists of using strip integrations through the thickness based on one point at the midsurface of the shell.

Three separate runs were conducted using DYNAPLAS. The first two were with 15 Fourier terms, 27 modified Simpson stations around the circumference but with and without the rotational degree of restraint at the fixed end. If membrane theory is adequate the rotational degree of restraint should not be important which was in fact found to

be the case. The 20 Fourier term analysis was conducted as the Fourier coefficients for the pressure load were converging very slowly. However, it should be recognized that the stiffnesses of the higher Fourier terms are quite large and thus a convergent series for the pressure loads is not necessary. For 15 Fourier terms and 27 stations around the circumference the computer run time was 53 minutes on the IBM 360/65. This is equivalent to approximately 13 minutes on the CDC 6600.

The results for the radial deflection and the meridional strain at the middle of the shell and at $\theta = 0$ are shown in Figs. 19 and 20 along with the results from REPSIL.²⁴ Needless to say the agreement is rather poor. More interesting is that DYNAPLAS predicts lower deflections but higher strains than predicted by REPSIL. To check the consistency of strains and deflections an elementary analysis was conducted. The deflection shape was assumed to be represented by

$$\omega = \frac{\delta}{2} \left(1 - \cos \frac{\pi\theta}{L/2} \right) \quad (78)$$

where δ is the deflection at the center. The average value of the strain was then computed by evaluating the deformed length, subtracting it from the undeformed length, and dividing by the undeformed length. The results based on the deflections obtained from DYNAPLAS are shown in Fig. 20. A check of the strains computed by DYNAPLAS reveal that the value of 20% is very close to the average value at the maximum load. Using the value of 2.5" for the maximum deflection

as obtained by REPSIL in Eq. 78 yields an average strain of 34%.

There are two differences in DYNAPLAS and REPSIL which may account for the differences in results for this highly nonlinear problem. First DYNAPLAS permits moderate rotations whereas REPSIL permits arbitrarily large rotations. Second REPSIL takes the pressure as acting normal to the deformed surface of the shell where DYNAPLAS uses the reference surface of the undeformed shell. This second point may be quite important for this problem. Underwood has agreed to study this problem and his results should be available before the results are published in the open literature.

Conical Frustum Under Half-Cosine Impulse

Since it was necessary to use partial membrane theory on the previous problem it was deemed necessary to show that the difficulty is caused by the thinness of the shell and not because of highly nonlinear behavior. For this purpose the previously studied conical frustum shell was again analyzed with the initial impulse being increased by a factor of 2.5. Results for deflections and strains are shown in Figs. 21, 22, and 23. Examination of the output data reveals deflections over $1/2$ of the average radius of the shell and strains as great as 40%. Seven Simpson stations were used through the thickness and a detailed study of the data revealed no oscillations in the rotations at the nodes.

Hypothetical Submarine

To illustrate the application of DYNAPLAS to a problem which involves a shell, stiffeners and springs, a structure with a vague resemblance to a submarine was chosen. Three different types of response are of interest. The first is due to a hydrostatic pressure followed by a high intensity transient load. The final stage of response is the overall vibration of the vehicle over a substantial period of time.

Except for the fluid-structure interaction, the total response is comparable to what might be encountered by a complex structural system, such as a submarine vehicle, subjected to hydrostatic pressures and shock environments. The application would prove extremely useful in the design and isolation of internal equipment subjected to shock loadings of such severity as to cause gross plastic deformation (but not complete failure) of the submarine hull.

In this example, the vehicle is 360" in length, 60" in diameter and has an intersecting vertical tube 12" in diameter. The material properties are typical of steel and are given in detail in the User's Manual for DYNAPLAS. The purpose of the present presentation is to present an overall view of the analysis procedure including some typical curves.

Ideally, the analysis would consist of inputting the detailed geometry of the complete vehicle and conducting the analysis. However this would require excessive computer run time and more storage than is available on most computers. For this reason the portion of the

vehicle around the tube was selected as the region of primary interest. The vehicle was idealized as shown in Fig. 24 with the element breakdown shown in Fig. 25. Six elements were used for the hemispherical nose and rather large elements were used for the stiffened cylinder except around the tube where 19 rather closely spaced elements were used as shown in Fig. 25b. It was assumed that the vehicle is symmetric about the centerline. A total of 45 finite elements were used in the idealization. Details of the geometry including the stiffeners are shown in Fig. 24.

The spring constants for the tube were determined based on elementary beam theory. These included both deflection and rotational springs. The detailed values for the spring constants are given in the User's Manual.

The hydrostatic solution for a uniform pressure of 500 psi was obtained by applying a linearly increasing pressure to a time of 20,000 μ sec and holding it constant at 500 psi to 50,000 μ sec. A time step of 1000 μ sec was used in the solution procedure. A slow application of the pressure was necessary as it was found that a step loading caused numerical instabilities when large time steps were used. These instabilities are believed to be due to the presence of the tube. Also it was necessary to apply a radial restraint at the apex to eliminate rigid body motion. It was found that the deflection increased linearly to 20,000 μ sec and remained constant thereafter. A check of the results shows a membrane solution for the hemispherical nose but variations of the stress near the stiffeners and the tube as would be expected. Five Fourier terms were used in the solution.

Next the boundary condition was removed and a high intensity pressure with a decay time of 40 μsec was applied to the shell in addition to the hydrostatic pressure. The pressure was assumed to vary as a half cosine around the circumference and to decrease as it approached the end of the vehicle. For this part of the analysis the program was restarted with a time step of 2 μsec and allowed to run for 120 μsec .

For the transient response it was assumed that the only region where plasticity and geometric nonlinearities were important was the area around the missile tube. A very high yield stress was used for the other elements and stiffeners and only a single modified Simpson station was used around the circumference.

To account for the overall response of the vehicle the code was restarted at 50,120 μsec with a time increment of 5 μsec and run to 50,320 μsec . Next it was restarted with a time step of 15 μsec and run to 51,400 μsec . In a separate restart at 50,320 μsec a time step of 50 μsec was used and the analysis was conducted to 55,000 μsec .

Results for the meridional strain near the tube are shown in Fig. 26. The distinct phases of the response to each of the different loads can be observed. First the hydrostatic value is reached and then a rapid increase occurs when the transient load is applied. The slight dip in the value of the strain when the transient load is applied is unexplained. The rest of the response is the vibration of the modes of the vehicle.

Two fundamental modes of vibration of the overall vehicle were

observed. The first is a lateral vibration similar to a free-free beam. This is depicted in Fig. 27 as the response of Fourier coefficient No. 1. The actual results showed appreciable lateral translation of the vehicle.

The other response which was easily observed is the response of the shell in a ring mode of vibration. An elementary calculation revealed that this mode has a period of 10,000 μ sec. The computations were not carried out to where this mode reaches its peak.

The purpose of this problem was to demonstrate that DYNAPLAS is capable of solving such complex problems and not to report a detailed analysis due to the assumptions in structure and loads. However it is concluded from this study that DYNAPLAS may be used for such analyses.

Cylindrical Panel

A cylindrical panel under an impulsively applied load was studied to determine if such problems can be solved by representing the boundaries by spring supports. The panel circumscribed an angle of only 60°. Analyses were conducted using 5, 10, 15, and 20 Fourier terms.

Results agree with experimental and other theoretical results up to near the peak deflection but DYNAPLAS results show considerable more "snap-back." A check of results shows that there are appreciable deflections in the shell beyond the spring supports. The conclusion reached from this study is that DYNAPLAS may be used for the initial response of panels but may not be used to study complete panel behavior unless the panel circumscribes almost 360° as was the case for the clamped ring under impulsive loading.

Users Hints

Recent convergence studies have shown that most results given in this report were not obtained in the most efficient manner. The following guidelines should save appreciably on computer run time.

1. For moderately nonlinear problems the psuedo forces should be updated every two or three time increments and an extrapolation factor of 1.0 should be used. For problems involving a high degree of geometric nonlinearities the psuedo forces must be updated every time cycle.

2. The number of modified Simpson's stations around the circumference may be less than the number of Fourier terms used.

3. Three to five Simpson's stations through the thickness should be adequate for most problems.

DYNAPLAS is currently being extended to provide the following:

1. Variable thickness in the circumferential direction.
2. Strain rate effects.
3. Temperature effects including the variations of material properties with temperature.
4. Improved plasticity relations including orthotropic plasticity.

Statement of Policy

The primary objective of this research is to develop a computer code which will be useful to the engineering community. Consistent with this objective the authors welcome comments from the users and are willing to assist the users within reason. This is especially true of users associated with the Navy, AEC, and NASA who have supported and continue to support this research and the many users of SNASOR II and DYNASOR II who have helped, through their comments, to make these better computer codes.

References

1. Argyris, J.H., Energy Theorems and Structural Analysis, Butterworths, London, 1960.
2. Atluri, S., Witmer, E.A., Leech, J.W., and Mornio, L., "PETROS 3: A Finite-Difference Method and Program for the Calculation of Large Elastic-Plastic Dynamically-Induced Deformations of Multilayer Variable-Thickness Shells." Massachusetts Institute of Technology, ASRL TR 152-2, (BRL CR 60), November 1971.
3. Balmer, H.A., "Improved Computer Programs - DEPROSS 1, 2, and 3 - to Calculate the Dynamic Elastic-Plastic Two-Dimensional Responses of Impulsively-Loaded Beams, Rings, Plates, and Shells of Revolution." Massachusetts Institute of Technology, ASRL TR 128-3, August 1965.
4. Balmer, H.A., and Witmer, E.A., "Theoretical-Experimental Correlation of Large Dynamic and Permanent Deformations of Impulsively - Loaded Unbonded Concentric Rings." AFFDL-TR-65-143, Aeroelastic and Structures Research Laboratory, Massachusetts Institute of Technology, November 1965.
5. Basdekas, N.L., "Dynamic Response of Non-Uniform Circular Cylindrical Shells Stiffened by Non-Uniform Rings." Ph.D. Dissertation, The Catholic University of America, Washington, D.C., June 1969.
6. Bathe, K.J., and Wilson, E.L., "Stability and Accuracy Analysis of Direct Integration Methods," To be published in International Journal of Earthquake Engineering and Structural Dynamics, April, 1973.
7. Biot, M.A., Mechanics of Incremental Deformations. John Wiley and Sons, 1965.
8. Birnbaun, M.R., Cupps, F.J., and Emery, A.F., "Spectre - A Finite Difference Computer Program For Calculating the Dynamic Response of A Cylindrical Shell," SCL-DR-70-108, Sandia Laboratories, Livermore, California, Dec. 1970.
9. Budiansky, B., and Radkowski, P.P., "Numerical Analysis of Unsymmetrical Bending of Shells of Revolution." AIAA Journal, Vol. 1, No. 8, August 1963, pp. 1833-1842.
10. Chan, S.P., Cox, H.L., and Benfield, W.A., "Transient Analysis of Forced Vibrations of Complex Structural-Mechanical Systems." J. Royal Aero. Soc., Vol. 66, No. 619, July 1962, pp. 457-460.

11. Chang, G.C., and Fair, G.S., "Finite Element Approach to Wave Motions in Elastic-Plastic Continua," Proc. AIAA 6th Aerospace Sciences Meeting, Paper 68-145, New York, Jan. 1968.
12. Chung, T.S., and Eidson, R.L., "Analysis of Viscoelasticplastic Structural Behavior of Anisotropic Shells by the Finite Element Method," Proceedings of First International Conference of Structural Mechanics in Reactor Technology, Berlin, Sept. 20-24, 1971.
13. Cohen, G.A., "Computer Analysis of Asymmetrical Buckling of Ring-Stiffened Orthotropic Shells of Revolution." AIAA Journal, Vol. 6, No. 1, January 1968, pp. 141-169.
14. Duffey, T., and Krieg, R., "The Effect of Strain-Hardening and Strain-Rate Sensitivity on the Transient Response of Elastic-Plastic Rings and Cylinders," Int. J. Mech. Sci., Vol. II, 1969, pp. 825-844.
15. Duffey, T.A., and Key, S.W., "Experimental-Theoretical Correlations of Impulsively Loaded Clamped Circular Plates," SC-RR-68-210, Sandia Laboratories, Albuquerque, New Mexico, April 1968.
16. Farhoomand, I., and Wilson, E.L., "A Nonlinear Finite Element Code for Analyzing the Blast Response of Underground Structure," Contract Report No. N-70-1 conducted for U.S. Army Engineer Waterways Experiment Station, Vicksburg, Miss., Jan. 1970.
17. Fung, Y.C., Foundations of Solid Mechanics. Prentice-Hall, 1965.
18. Haisler, W.E., Jr., "Development and Evaluation of Solution Procedures for Nonlinear Structural Analysis," Ph.D. Dissertation, December 1970, Texas A&M University, College Station, Texas.
19. Haisler, W.E., and Stricklin, J.A., "Nonlinear Finite Element Analysis Including Higher-Order Strain Energy Terms." AIAA Journal, Vol. 8, No. 6, June 1970, pp. 1158-1159.
20. Hill, R., Mathematical Theory of Plasticity, Clarendon Press, Oxford, 1950.
21. Houbolt, J.C., "A Recurrence Matrix Solution for the Dynamic Response of Elastic Aircraft." Journal of the Aero. Sciences, Vol. 17, 1950, pp. 540-550.
22. Hubka, W.F., "A Calculation Method for the Finite Deflection, Elastic-Plastic Dynamic Response of Shells of Revolution." Kaman Nuclear Report No. KN-69-26(M), January 1969.

23. Huffington, N.J., Jr., Private correspondence pertaining to REPSIL computer code, July 1972.
24. Huffington, N.J., Jr., "Large Deflection Elastoplastic Response of Shell Structures". Report No. 1515, Ballistic Research Laboratories, Aberdeen Proving Ground, Maryland, 1970.
25. Huffington, N.J., Jr., "Numerical Analysis of Elastoplastic Stress." U.S. Army Ballistic Research Laboratory, Memorandum Report No. 2006, September 1969.
26. Jones, N., "The Influence of a Rigid Viscoplastic Strain-Hardening Annular Plate Loaded Impulsively." Report No. 68-21, Department of Naval Architecture and Marine Engineering, Massachusetts Institute of Technology, Cambridge, Mass., Nov. 1968.
27. Kalnins, A., "Static, Free Vibration, and Stability Analysis of Thin Elastic Shells of Revolution." Air Force Flight Dynamic Laboratory Report, AFFDL-TR-68-144, March 1969.
28. Key, S.W., and Beisinger, Zelma E., "The Transient Dynamic Analysis of Thin Shells by the Finite Element Method," presented at Air Force Third Conference on Matrix Methods in Structural Mechanics, Wright-Patterson Air Force Base, Ohio, Oct. 19-21, 1971.
29. Key, S.W., Krieg, R.D., "Comparison of Finite Element and Finite Difference Methods," Sandia Corporation, SC-DC-713890, International Symposium on Numerical and Computer Methods in Structural Mechanics, Urbana, Illinois, September 8-10, 1971.
30. Klein, S., and Sylvester, R.J., "The Linear Elastic Dynamic Analysis of Shells of Revolution by the Matrix Displacement Method." Proceedings of the First AFFDL Conference in Matrix Methods in Structural Mechanics, AFFDL-TR-66-80, December 1968, pp. 299-328.
31. Krieg, R.D., Duffey, T.A., and Key, S.W., "The Large Deflection Elastic-Plastic Response of Impulsively-Loaded Beams - A Comparison Between Computations and Experiment." Sandia Laboratory, Albuquerque, New Mexico, Report SC-RR-68-226, July 1968.
32. Krieg, R.D., and Duffey, T.A., "UNIVALVE II: A Code to Calculate the Large Deflection Dynamic Response of Beams, Rings, Plates, and Cylinders." Sandia Corporation, Report SC-RR-68-303, October 1968.
33. Krieg, R.D., and Key, S.W., "Transient Shell Response by Numerical Time Integration," Proceedings of 2nd U.S. - Japan Seminar on Matrix Methods of Structural Analysis, University of Alabama Press, Huntsville, Alabama, 1972.

34. Leech, J.W., Witmer, E.A., and Pian, T.H.H., "Numerical Calculation Technique for Large Elastic-Plastic Transient Deformations of Thin Shells." AIAA Journal, Vol. 6, No. 12, Dec. 1968, pp. 2352-2359.
35. Lindberg, H.E., and Sliter, G.E., "Response of Re-entry Vehicle Type Shells to Transient Surface Pressures," Stanford Research Institute TR NO. AFWL-TR-68-56, Menlo Park, California, June 1969.
36. McNamara, J.F., and Marcal, P.V., "Incremental Stiffness Method for Finite Element Analysis of Nonlinear Dynamic Problems," Paper presented at International Symposium of Numerical and Computer Methods in Structural Mechanics, Urbana, Illinois, September 1971.
37. Mallett, R.H., and Marcal, P.V., "Finite Element Analysis of Non-linear Structures," Journal of the Structural Division, ASCE, Vol. 94, No. ST9, September 1968, pp. 2081-2105.
38. Marcal, P.V., "Large Deflection Analysis of Elastic-Plastic Shells of Revolution," AIAA/ASME 10th Structures, Structural Dynamics and Materials Conference, New Orleans, April 14-16, 1969.
39. Morino, L., Leech, J.W., and Witmer, E.A., "An Improved Numerical Calculation Technique for Large Elastic-Plastic Transient Deformations of Thin Shells." Journal of Applied Mechanics, Vol. 38, No. 2, June 1971, pp. 423-436.
40. Mroz, Z., "On the Description of Anisotropic Workhardening," J. Mech. Phys. Solids, Vol. 15, (1967), pp. 163-175.
41. Newmark, N.M., and Chan, S.P., "A Comparison of Numerical Methods for Analyzing Dynamic Response of Structures." Univ. of Illinois, Civil Engineering Structural Research Series 36, October 1952.
42. Newmark, N.M., "A Method of Computation for Structural Dynamics." Journal of the Engineering Mechanics, Div., Proceedings of the Am. Soc. of Civil Engr., Vol. 85, July 1959, pp. 67-94.
43. Nickell, R.E., "A Survey of Direct Integration Methods in Structural Dynamics," Report N00014-0007/9, Division of Engineering, Brown University, Providence, R.I., April 1972.
44. Nickell, R.E., "On the Stability of Approximation Operators in Problems of Structural Dynamics." Bell Telephone Laboratories, Tech. Memo 69-4116-14, Whippany, New Jersey, Nov. 1969 (also Int'l J. Solids and Structures, Vol. 7, 1971, pp. 301-319.

45. Novozhilov, V.V., Foundations of the Nonlinear Theory of Elasticity. Graylock Press, 1963.
46. Oden, J.T., and Kubitza, W.K., "Numerical Analysis of Nonlinear Pneumatic Structures," Proceedings of the First International Colloquium on Pneumatic Structures, Stuttgart, Germany, 1967.
47. Perrone, N., "Response of Rate-Sensitive Flows to Impulsive Load," J. Eng. Mech. Div., ASCE, EM1, Feb. 1971, pp. 49-62.
48. Perrone, N., and El. Kasrawy, T., "Dynamic Response of Pure-Loaded Rate Sensitive Structure," Int. J. Solid Structures, 1968, Vol. 4, pp. 517-530.
49. Stricklin, J.A., Martinez, J.E., Tillerson, J.R., Hong, J.H., and Haisler, W.E., "Nonlinear Dynamic Analysis of Shells of Revolution by the Matrix Displacement Method." AIAA Journal, Vol. 9, No. 4, April 1971, pp. 629-636.
50. Stricklin, J.A., Haisler, W.E., and Von Rieseemann, W.A., "Computation and Solution Procedures for Nonlinear Analysis by Combined Finite Element-Finite Difference Methods," Presented at the National Symposium on Computerized Structural Analysis and Design, George Washington University, Washington, D.C., March 27-29, 1972.
51. Stricklin, J.A., Haisler, W.E., and Von Rieseemann, W.A., "Formulation, Computation, and Solution Procedures for Material and/or Geometric Nonlinear Structural Analysis by the Finite Element Method," SC-CR-72-3102, Sandia Laboratories, Albuquerque, New Mexico, Jan. 1972.
52. Santiago, J.M., "Formulation of the Large Deflection Shell Equations for Use in Finite Difference Structural Response Computer Codes," Report No. 1571, Ballistic Research Laboratories, Aberdeen Proving Ground, Maryland, 1972.
53. Stricklin, J.A., Navaratna, D.R., and Pian, T.H.H., "Improvements on the Analysis of Shells of Revolution by the Matrix Displacement Method," AIAA Journal, Vol. 4, No. 11, Nov. 1966, pp. 2069-2072.
54. Stricklin, J.A., Martinez, J.E., Tillerson, J.R., Hong, J.H., and Haisler, W.E., "Nonlinear Dynamic Analysis of Shells of Revolution by the Matrix Displacement Method," Dept. of Aerospace Engr., Texas A&M University, Report 69-77, Feb. 1970.
55. Svalbonas, V., and Agrisano, N., "Numerical Analysis of Shells - Vol. II: User's Manual for Stars II - Shell Theory Automated for Rotational Structures." Grumman Aircraft Engineering Corp., Report No. FSR-AD2-01-68.5, August 1968.

56. Turner, M.J., Dill, E.H., Martin, H.C., and Melosh, R.J., "Large Deflection Analysis of Complex Structures Subjected to Heating and External Loads." J. Aero Space Sciences, Vol. 27, No. 2, Feb. 1960, pp. 97-106.
57. Underwood, P., "Transient Response of Inelastic Shells of Revolution," presented at National Symposium on Computerized Structural Analysis and Design, George Washington University, Washington D.C., March 1972.
58. Washizu, K., Variational Methods in Elasticity and Plasticity. Pergamon Press Ltd., 1968.
59. Wilson, E.L., "A Computer Program for the Dynamic Stress Analysis of Underground Structures." University of California, Berkeley, Report SEL-68-1, January 1968.
60. Witmer, E.A., Balmer, H.A., Leech, J.W., and Pian, T.H.H., "Large Dynamic Deformations of Beams, Rings, Plates, and Shells," AIAA Journal, Vol. 1, No. 8, August 1963, pp. 1848-1857.
61. Wrenn, B.G., Sobel, L.H., and Silsby, W., "Nonsymmetric and Nonlinear Response of Thin Shells: Lockheed Missiles and Space Co., Palo Alto, California, Report LMSC-B-72-67-3, December 1967.
62. Wu, R.W.H., and Witmer, E.A., "Finite-Element Analysis of Large Transient Elastic-Plastic Deformations of Simple Structures, with Application to the Engine Rotor Fragment Containment/Deflection Problem," NASA-CR-120886, National Aeronautics and Space Administration, Washington D.C., (Also ASRL TR 154-4.) Jan. 1972.
63. Wu, R.W.H., and Witmer, E.A., "Finite-Element Analysis of Large Elastic-Plastic Transient Deformations of Simple Structures." AIAA Journal, Vol. 9, No. 9, September 1971, pp. 1719-1724.
64. Yamada, Y., Kawai, T., Yoshimura, N., and Sakurai, T., "Analysis of the Elastic-Plastic Problem by the Matrix Displacement Method," Proceedings of the Second Conference on Matrix Methods in Structural Mechanics, Wright-Patterson Air Force Base, Ohio, Oct. 15-17, 1968. AFFDL-TR-68-150, December 1969, pp. 1271-1299.
65. Ziegler, H., "A Modification of Prager's Hardening Rule," Quarterly of Applied Mathematics, Vol. 17, No. 1, 1959, p. 55.

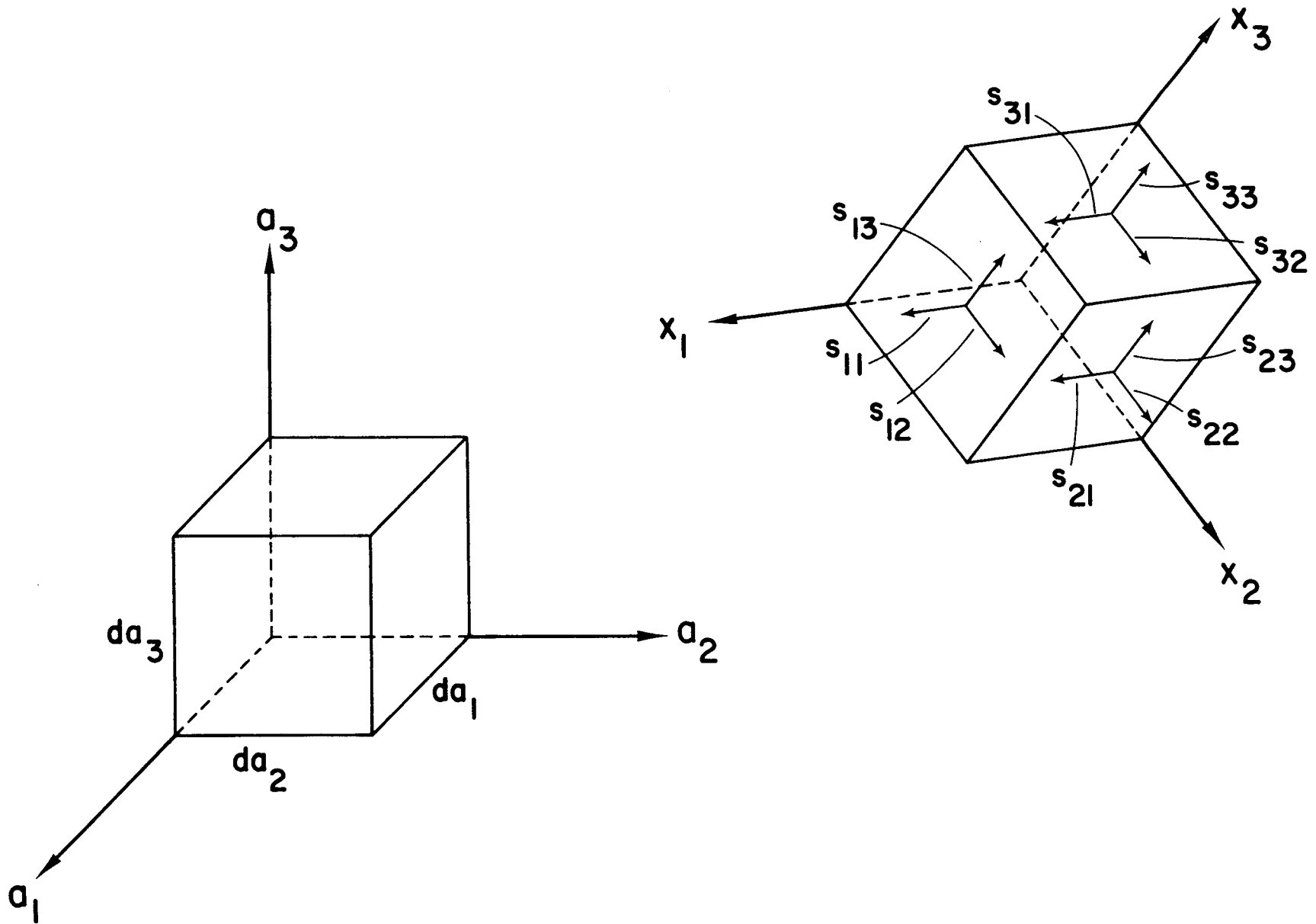


FIG.1 DIRECTIONS OF KIRCHHOFF STRESS

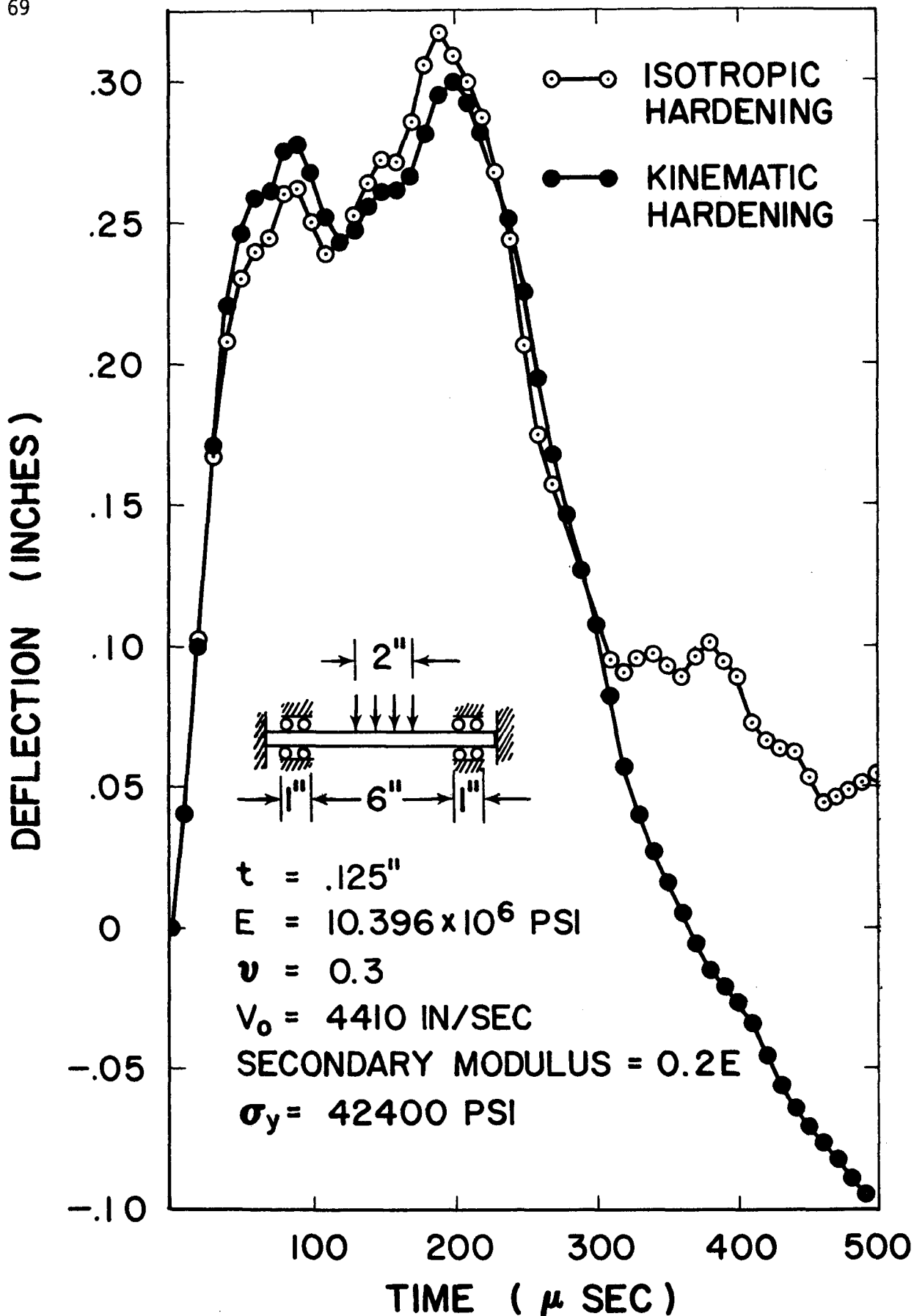
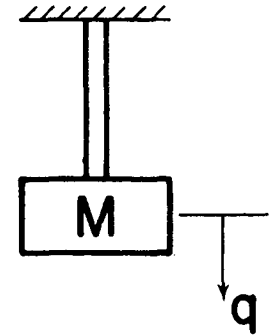
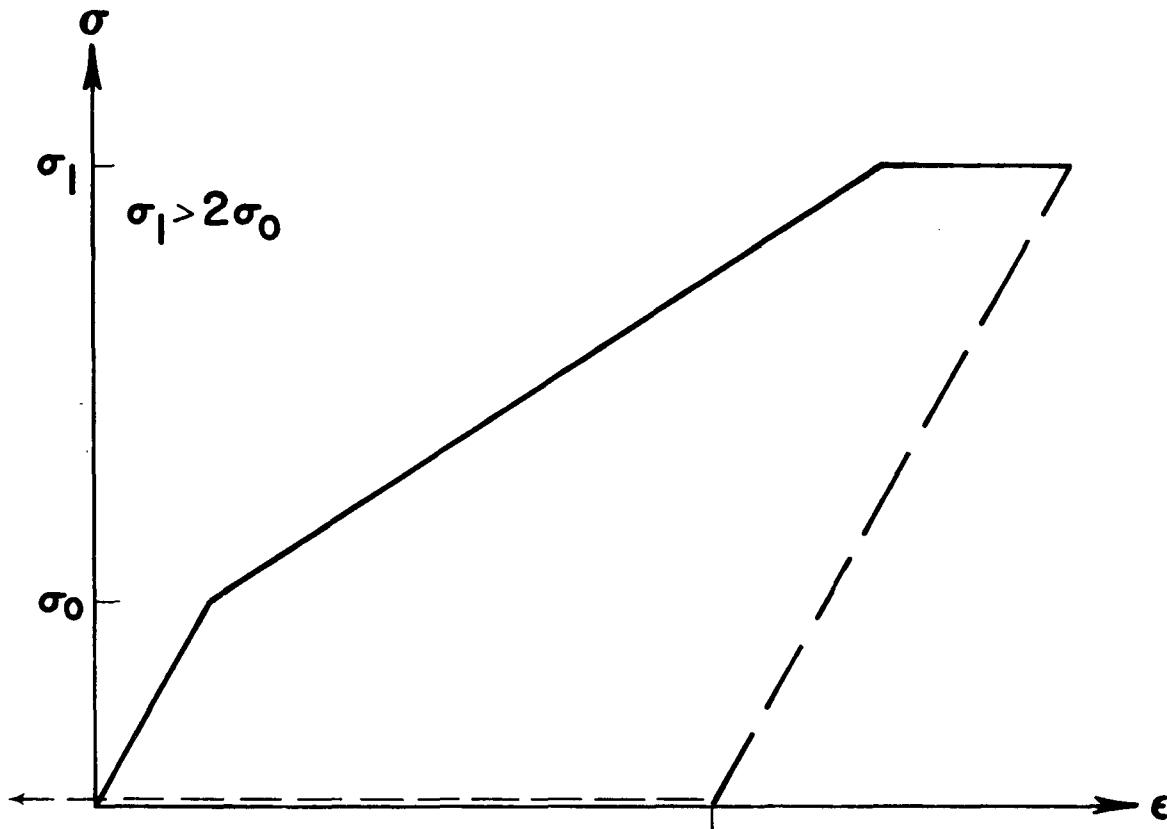


FIG. 2 CENTER DEFLECTION VS TIME FOR CIRCULAR PLATE



Final Strain
Kinematic Hardening

Final Strain
Isotropic Hardening

FIG. 3 DYNAMIC RESPONSE OF SIMPLE MASS

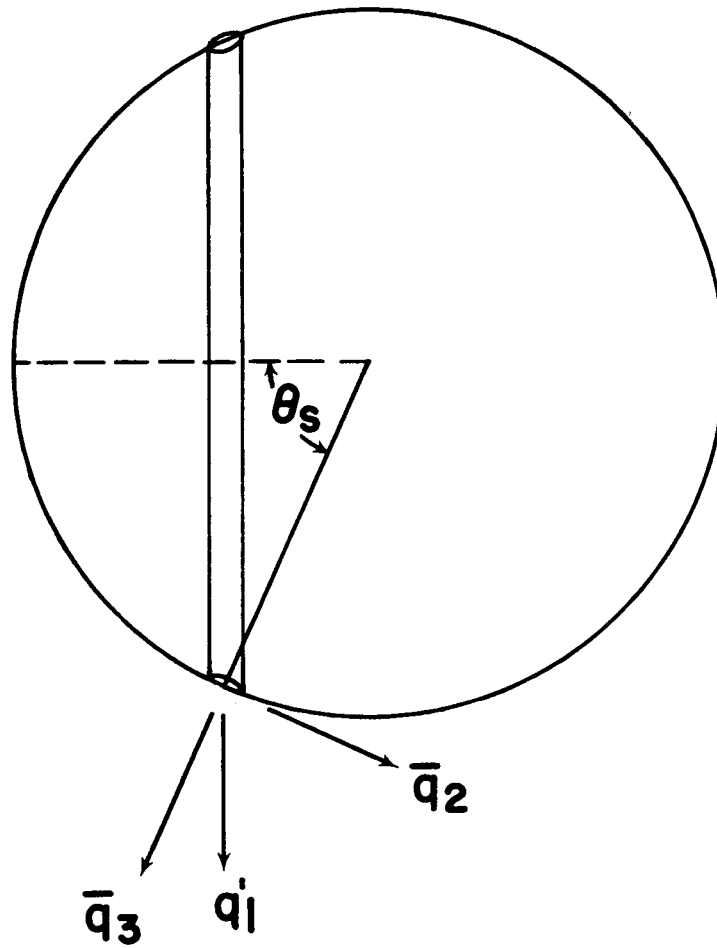


FIG. 5 SUPPORT ON CYLINDRICAL RING

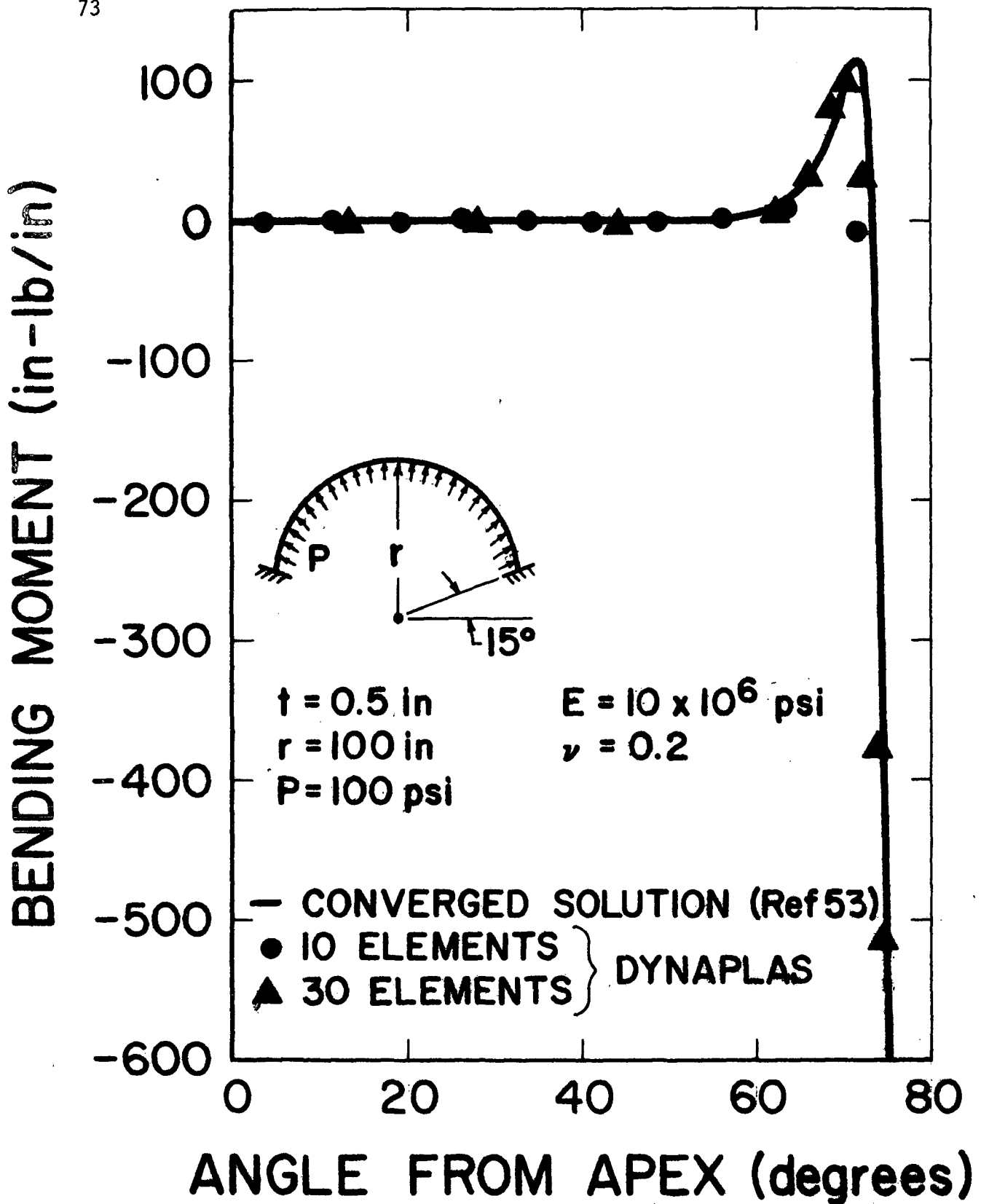


FIG. 6 MERIDIONAL BENDING MOMENT vs. ANGLE FROM APEX FOR A SPHERICAL CAP

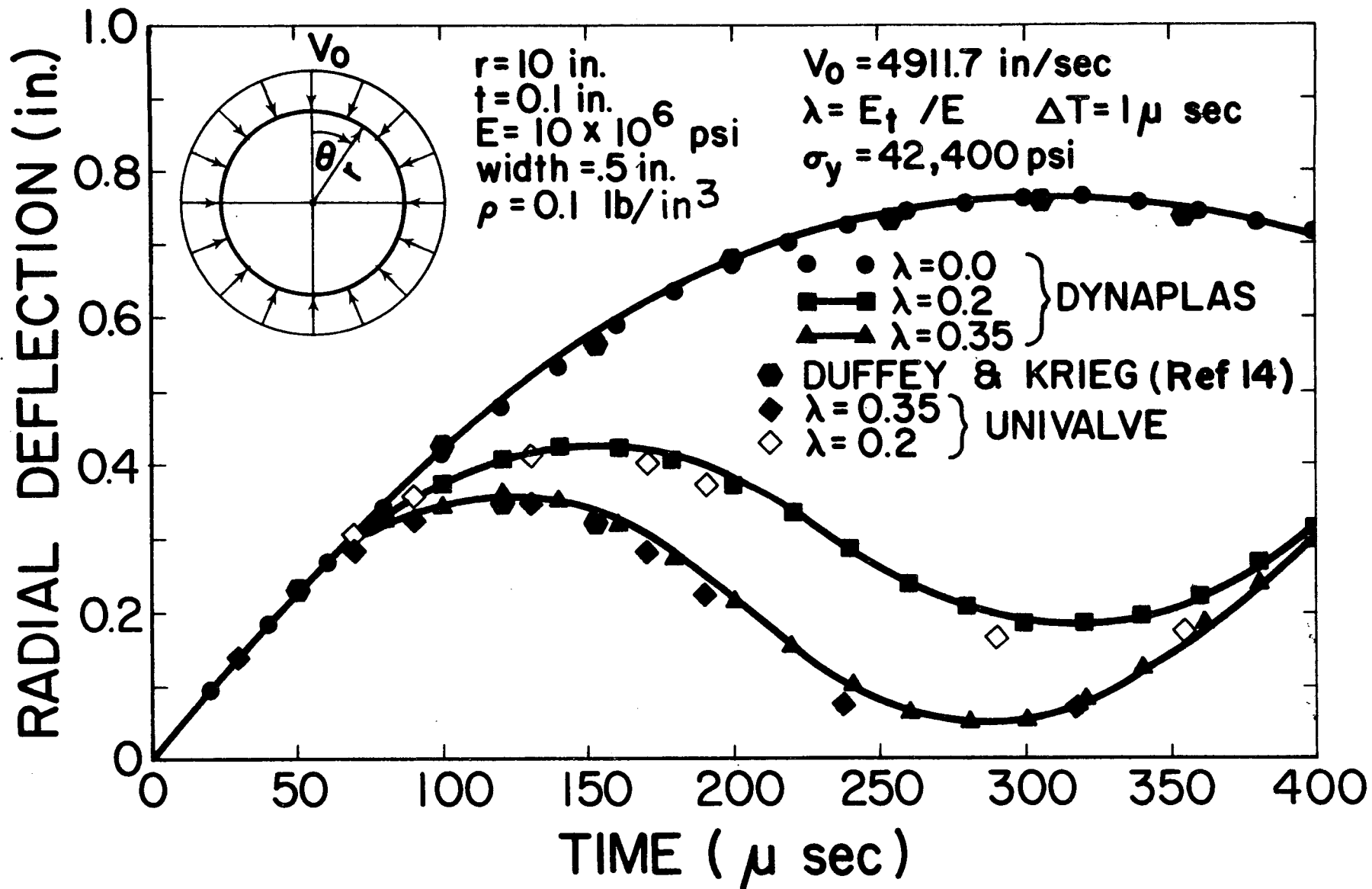


FIG. 7 RADIAL DISPLACEMENT FOR VARIOUS VALUES OF THE STRAIN-HARDENING PARAMETER, λ

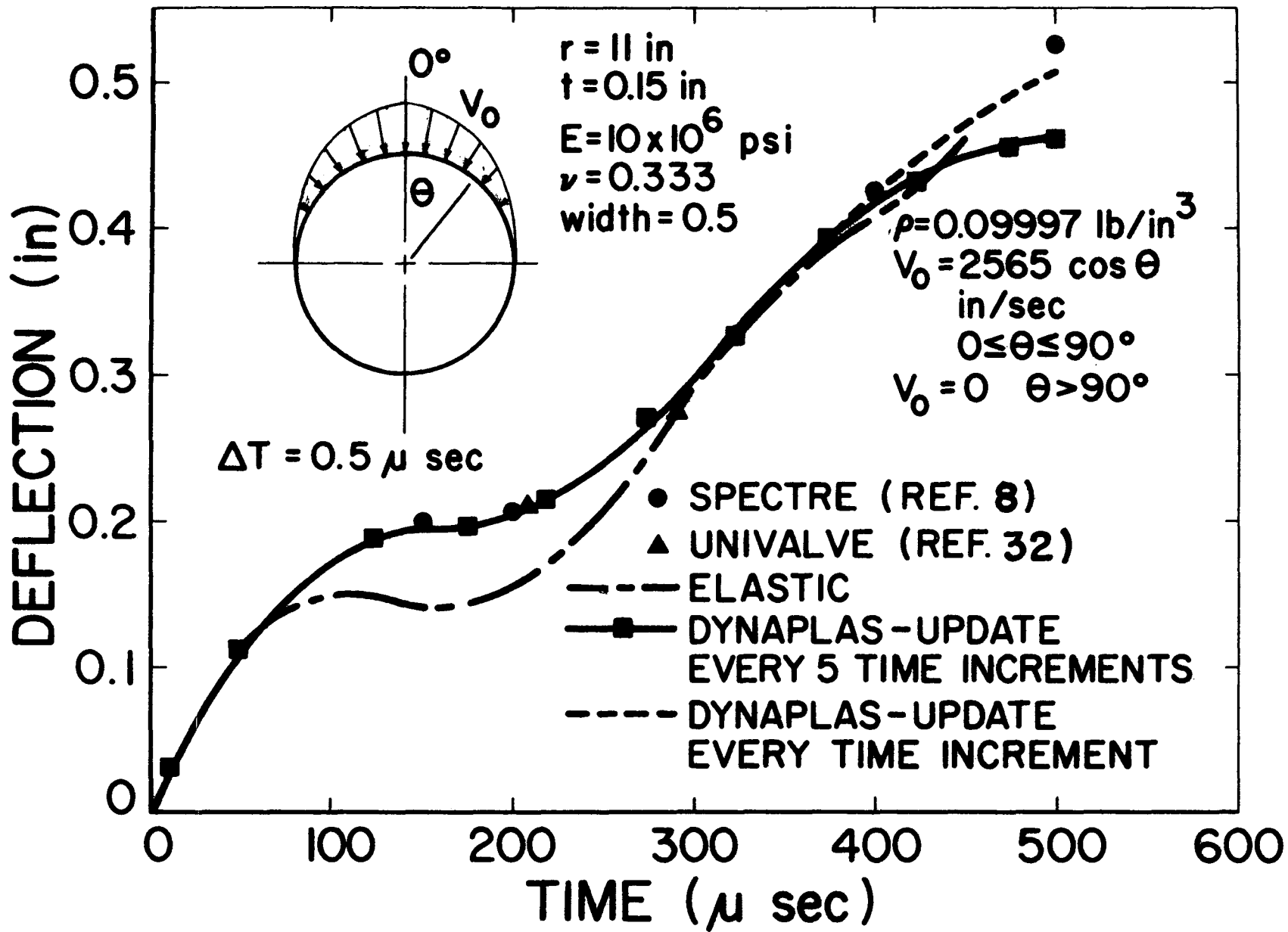


FIG. 8 RADIAL DISPLACEMENT AT THETA=0°

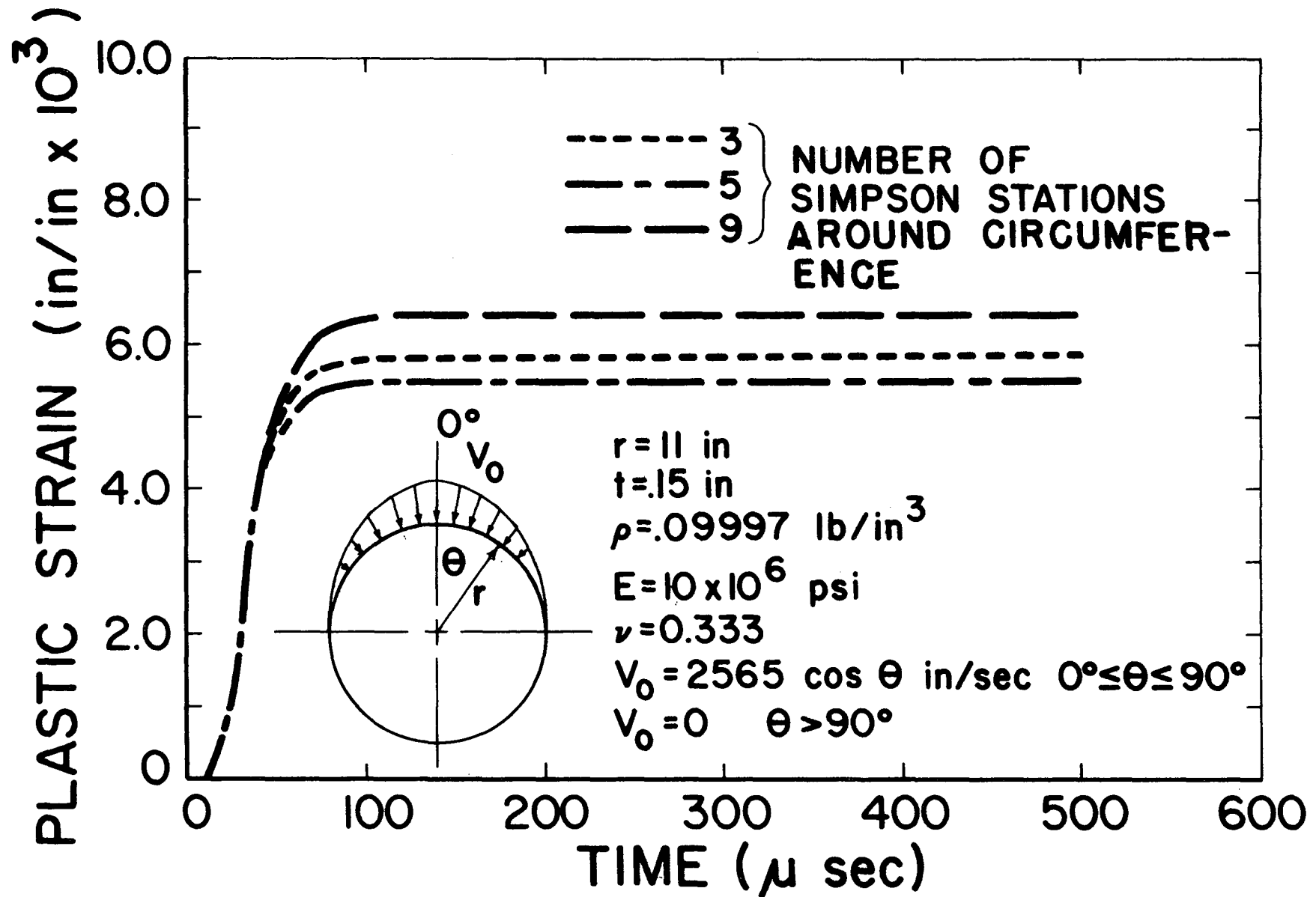


FIG. 9 PLASTIC STRAIN AT OUTER SURFACE AND $\theta = 0^\circ$ VERSUS TIME

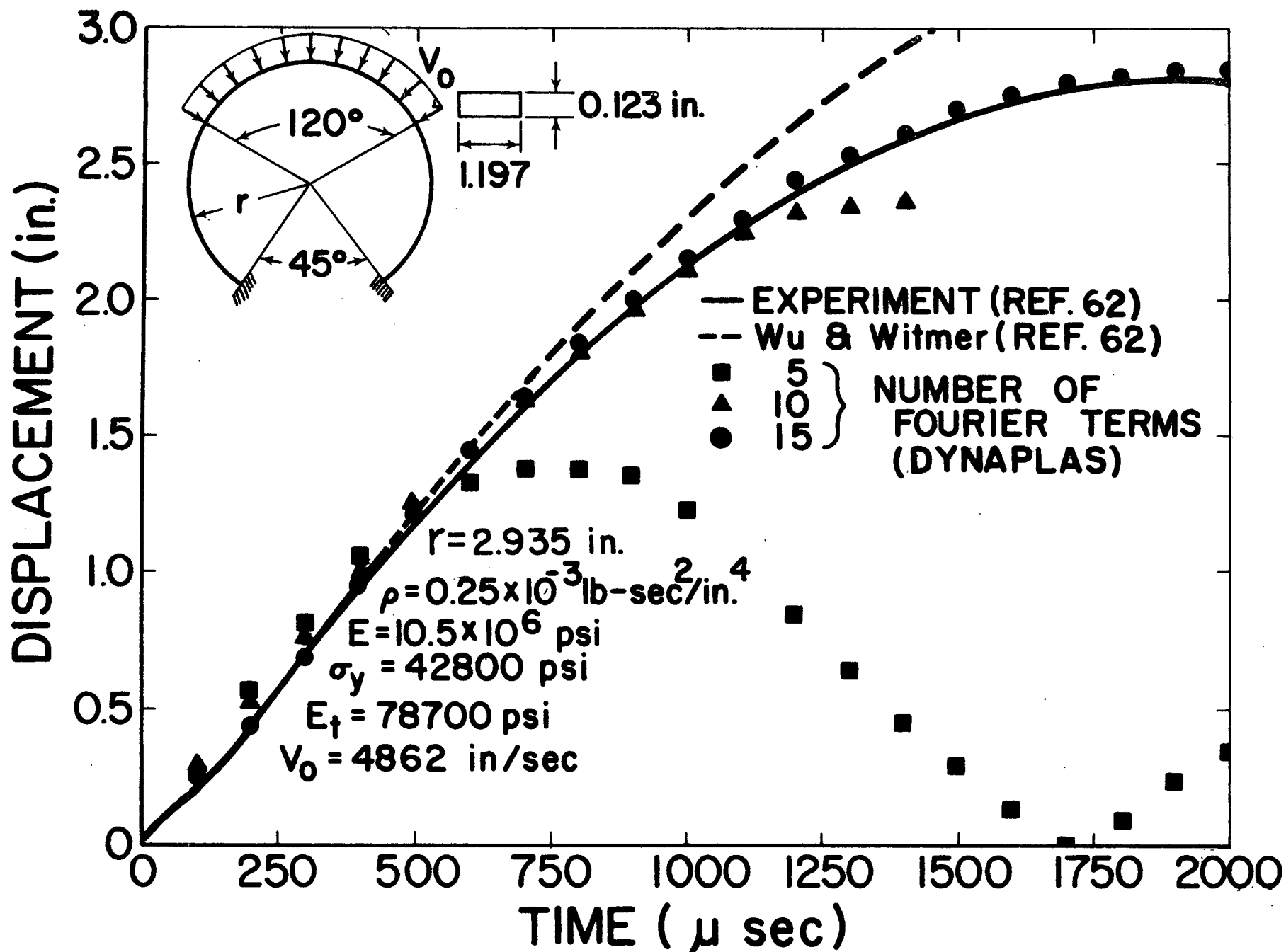


FIG. 10 RADIAL DISPLACEMENT AT THETA = 0.0°

CIRCUMFERENTIAL STRAINS

(in/in)

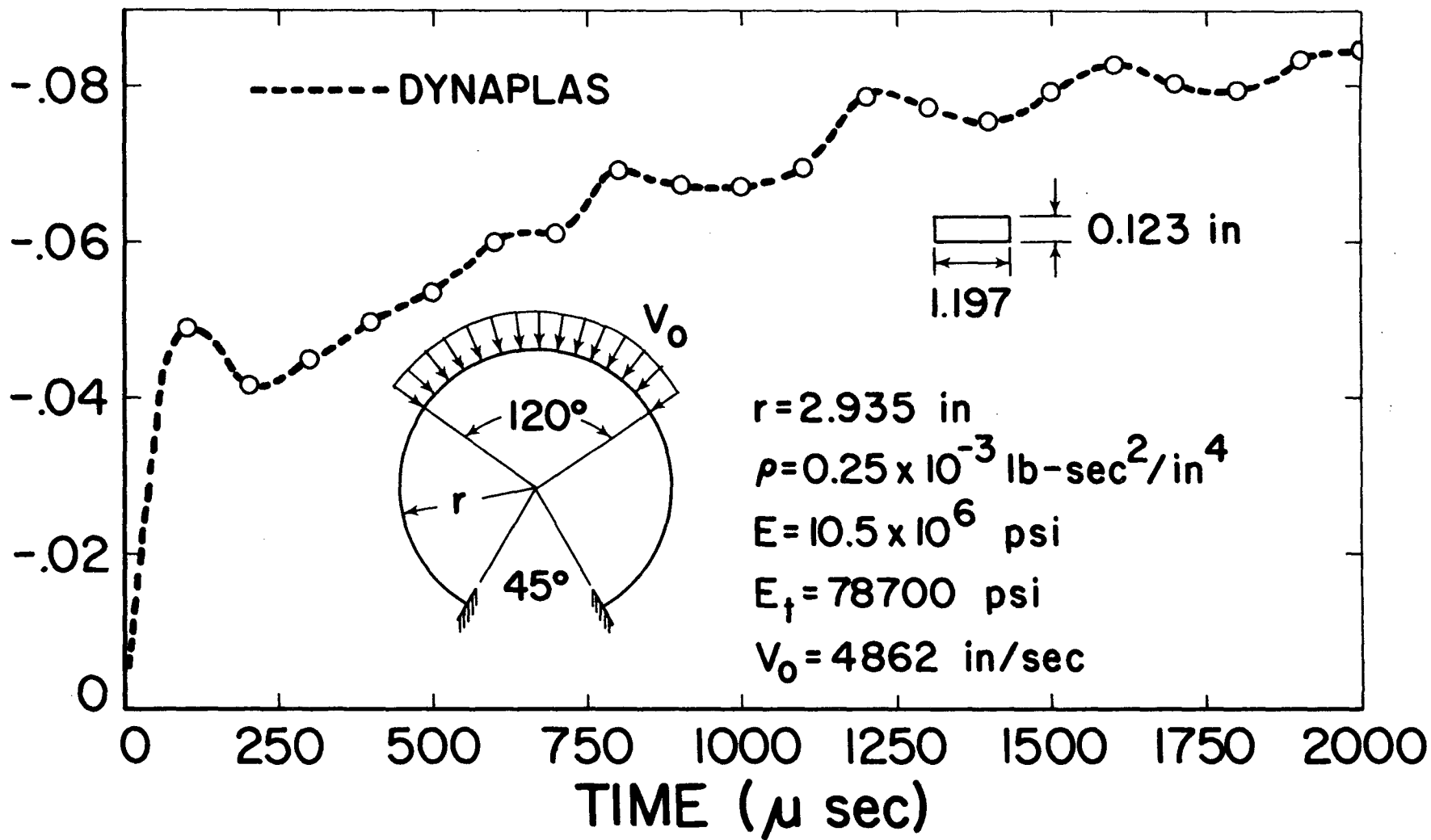


FIG. II CIRCUMFERENTIAL STRAIN AT THETA = 0.0° ON THE OUTER SURFACE

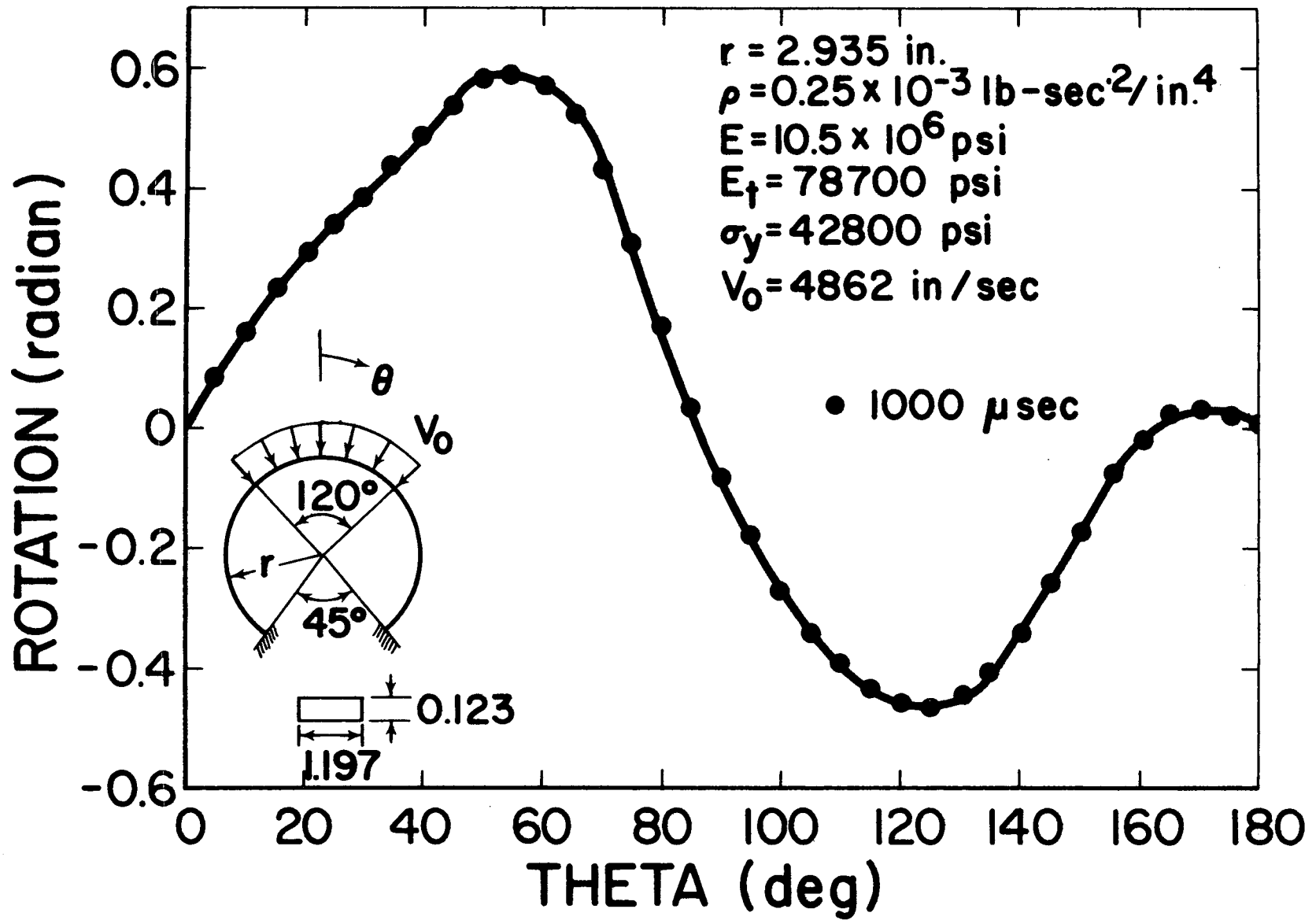


FIG. 12 ROTATION OF A CLAMPED RING

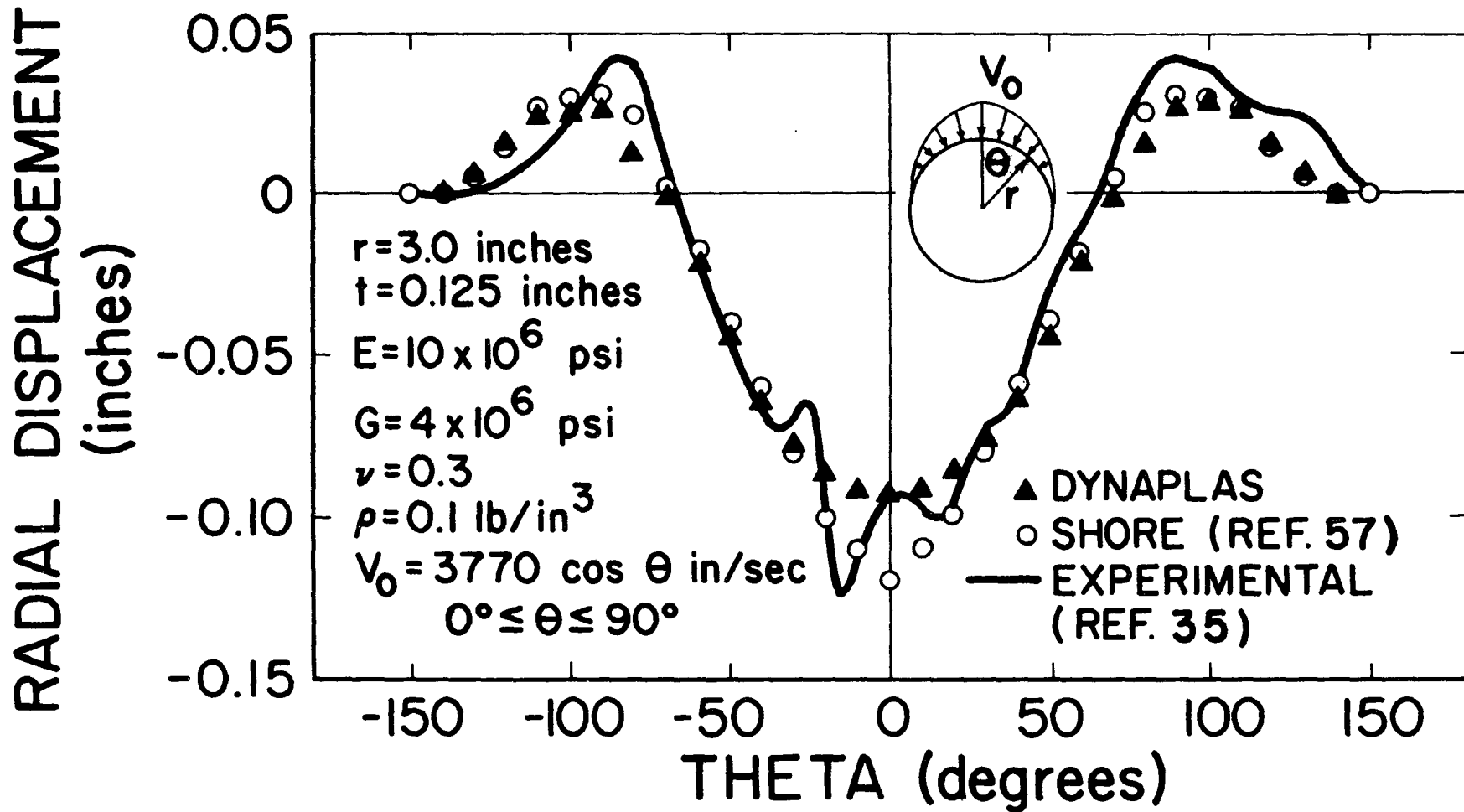


FIG. 13 RADIAL DISPLACEMENT AROUND THE CIRCUMFERENCE AT L/2

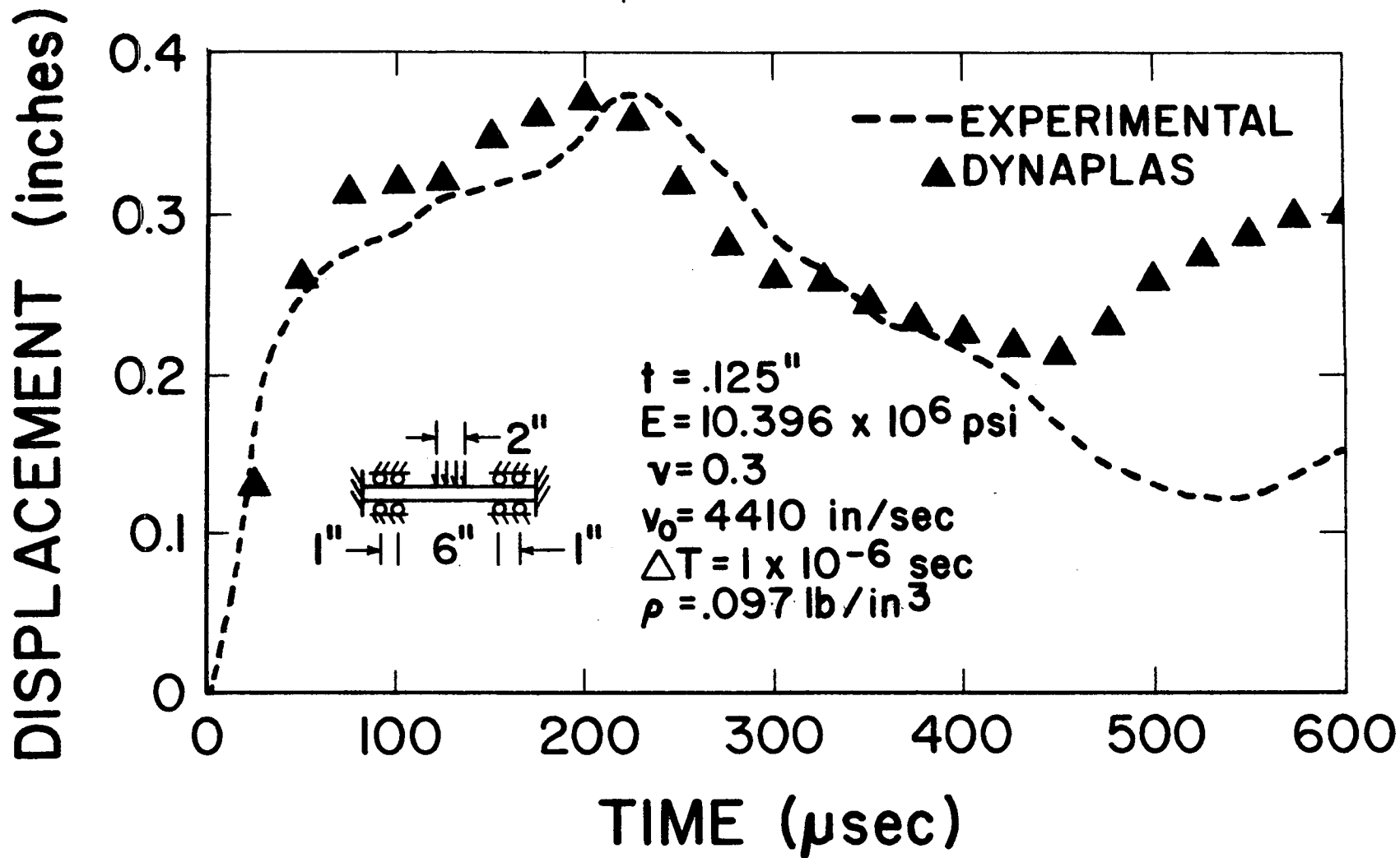


FIG 14 CENTER DEFLECTION vs TIME FOR AN IMPULSIVELY LOADED CIRCULAR PLATE

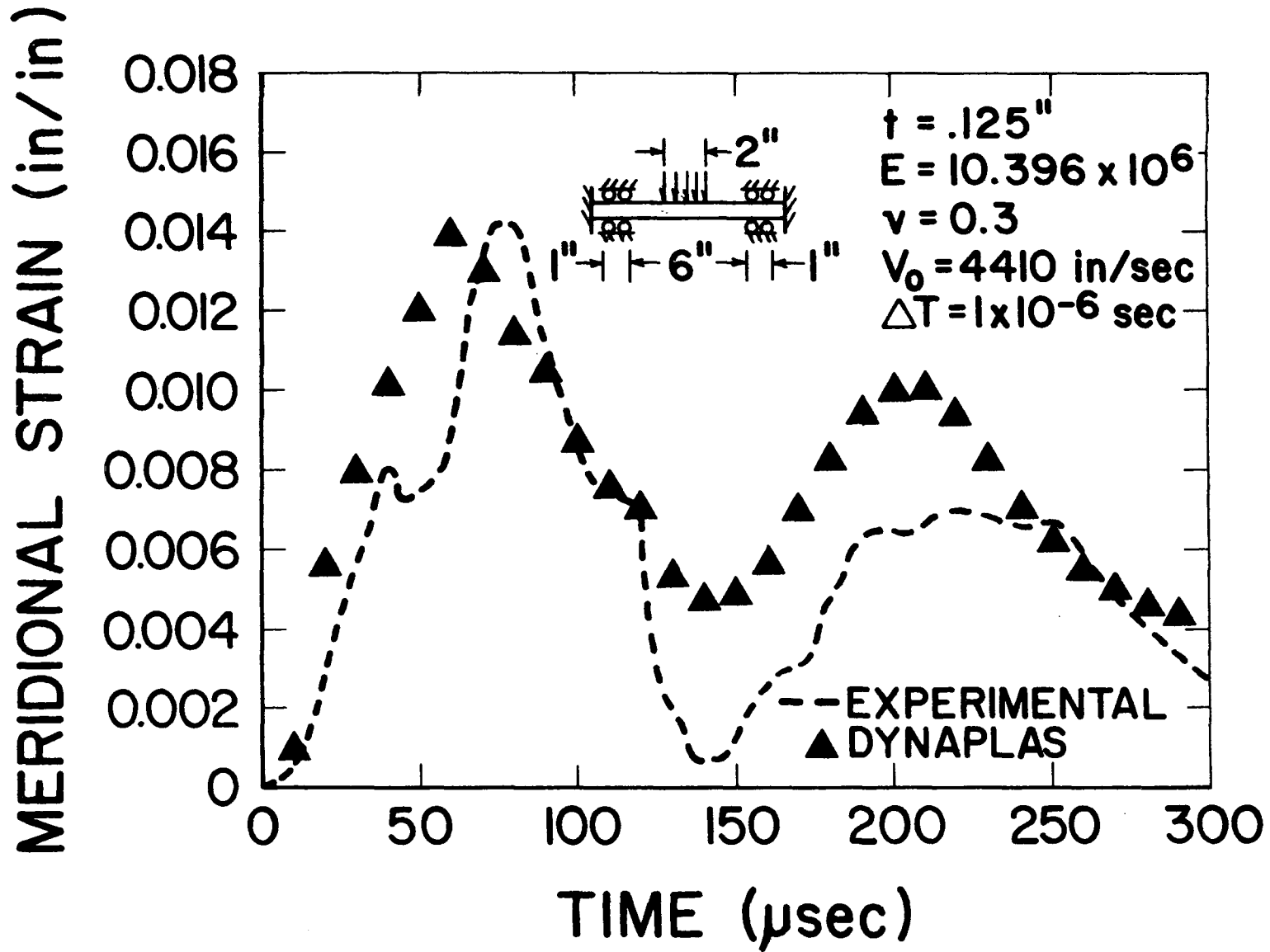


FIG 15 MERIDIONAL STRAIN ON TOP AT RADIUS OF 2.125 in

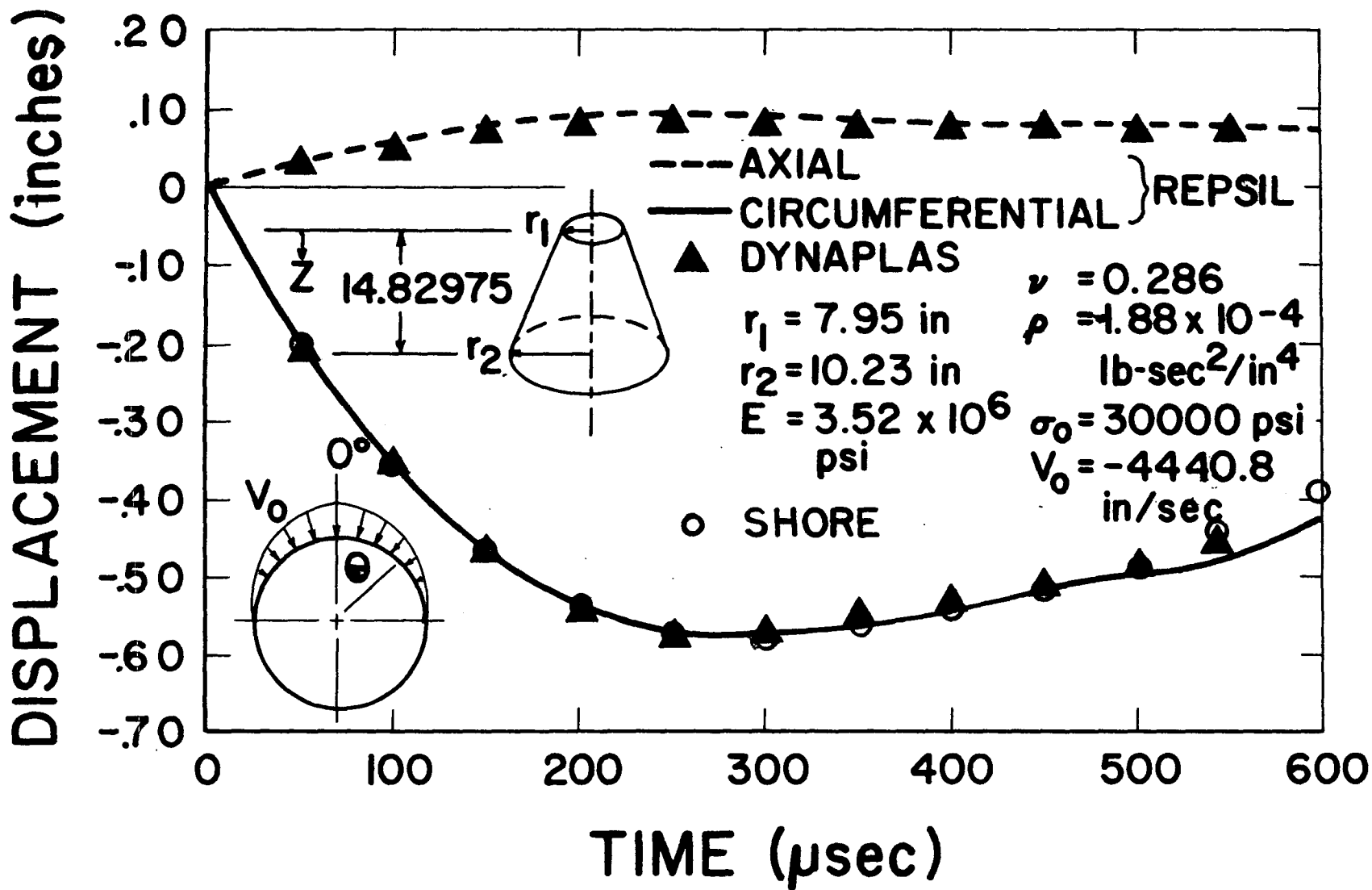


FIG 16 AXIAL AND RADIAL DISPLACEMENT FOR THETA=0° AND Z=6.3516 in

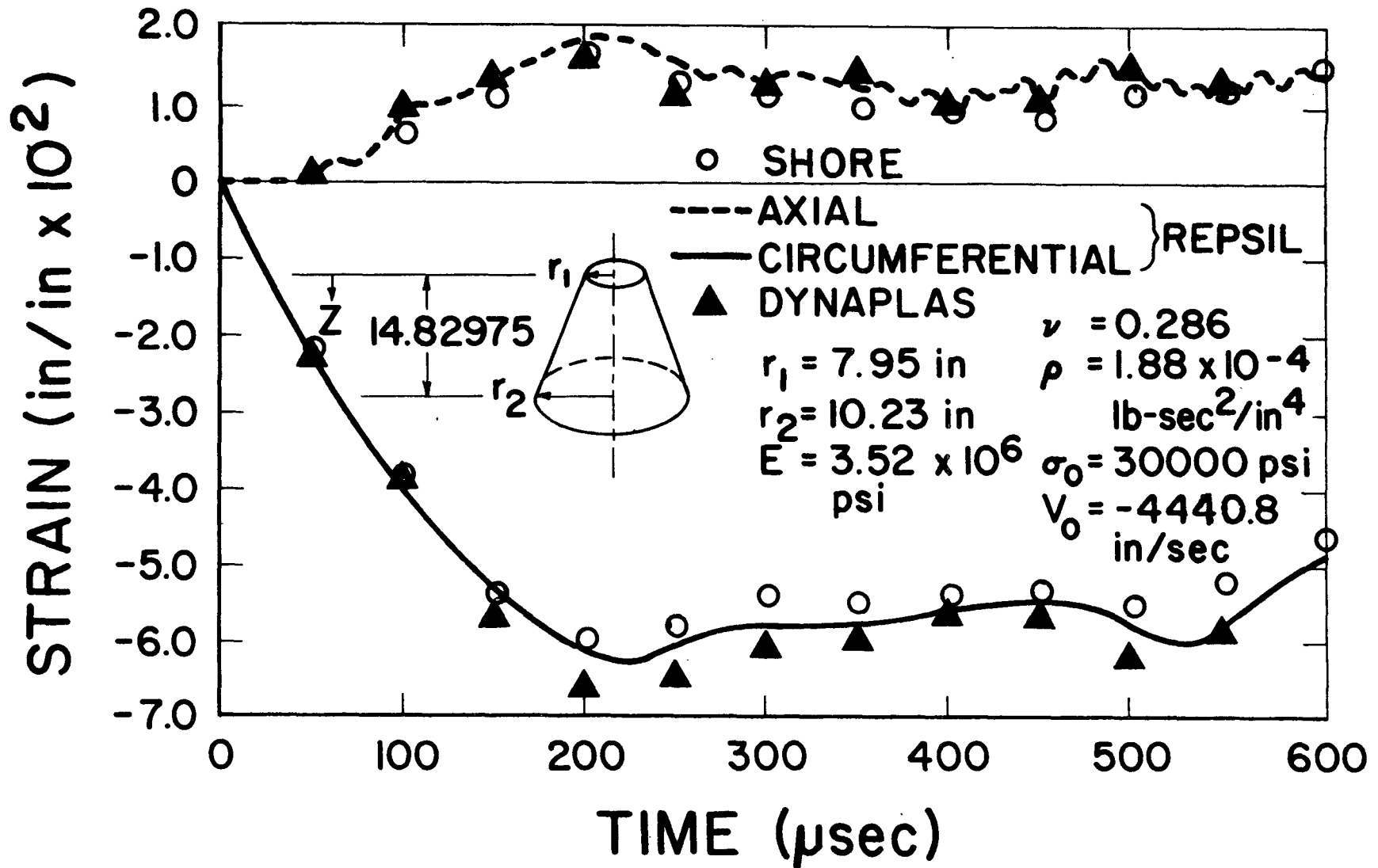


FIG.17 AXIAL AND CIRCUMFERENTIAL STRAIN
 AT THETA = 0° AND Z = 6.3516 in
 (OUTER SURFACE)

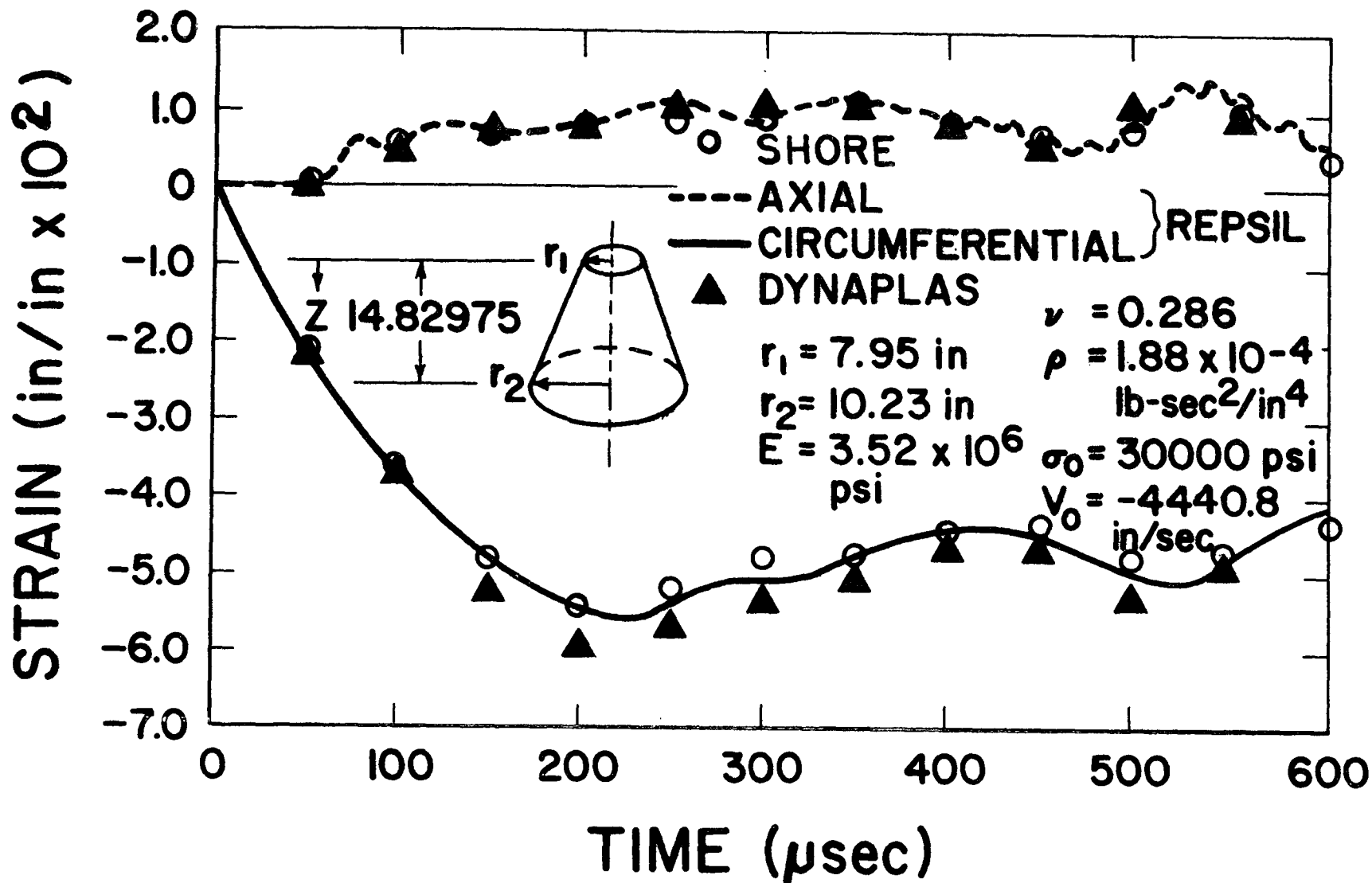


FIG.18 AXIAL AND CIRCUMFERENTIAL STRAIN
 AT THETA = 0° AND $Z = 6.3516$ in
 (INNER SURFACE)

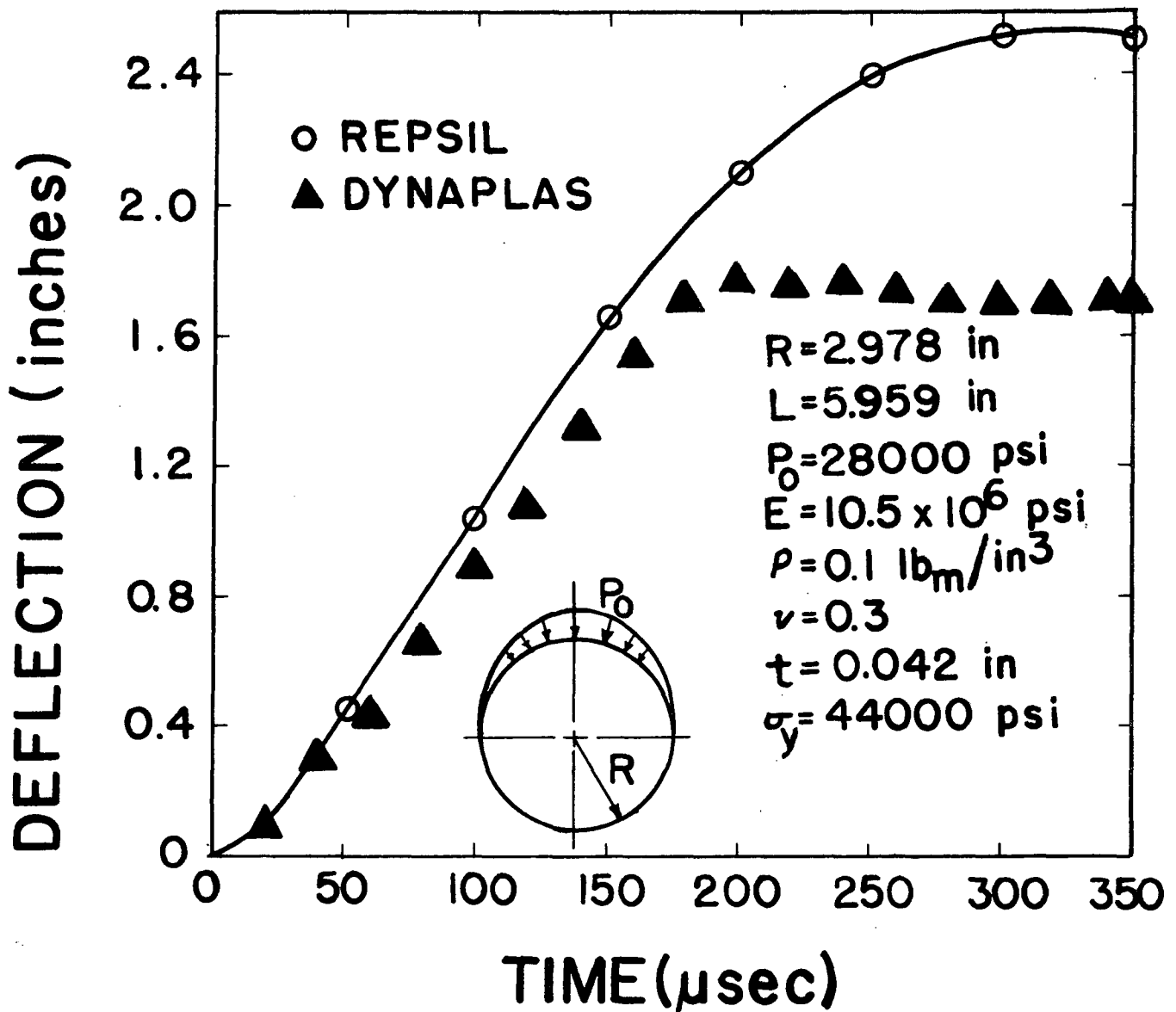


FIG. 19 DEFLECTION AT THETA=0° AND Z=L/2 FOR A CYLINDER SUBJECTED TO A MOVING PRESSURE LOAD

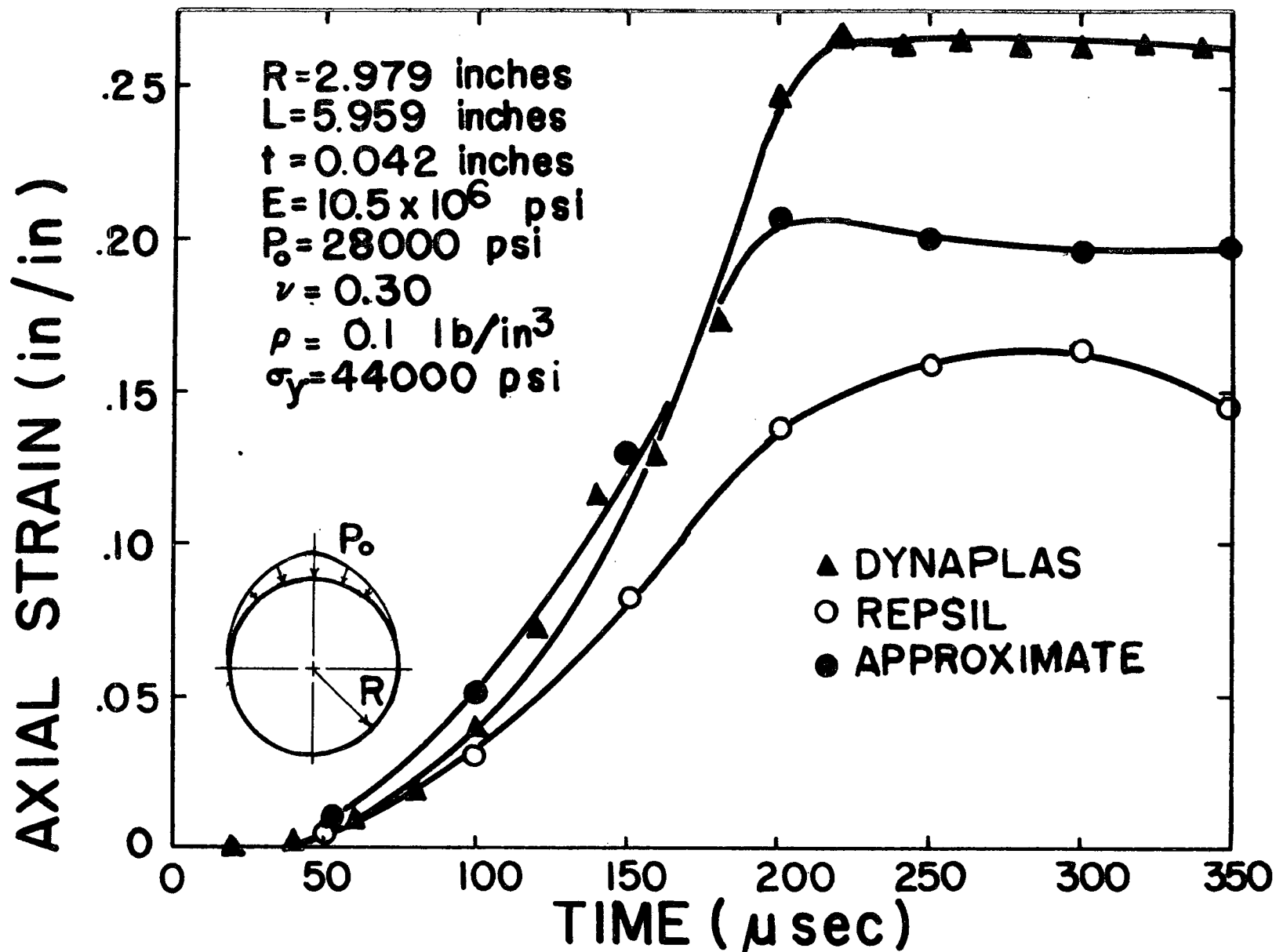


FIG. 20 MIDSURFACE AXIAL STRAIN AT THETA=0° AND Z=L/2 FOR A CYLINDER SUBJECTED TO A MOVING PRESSURE LOAD

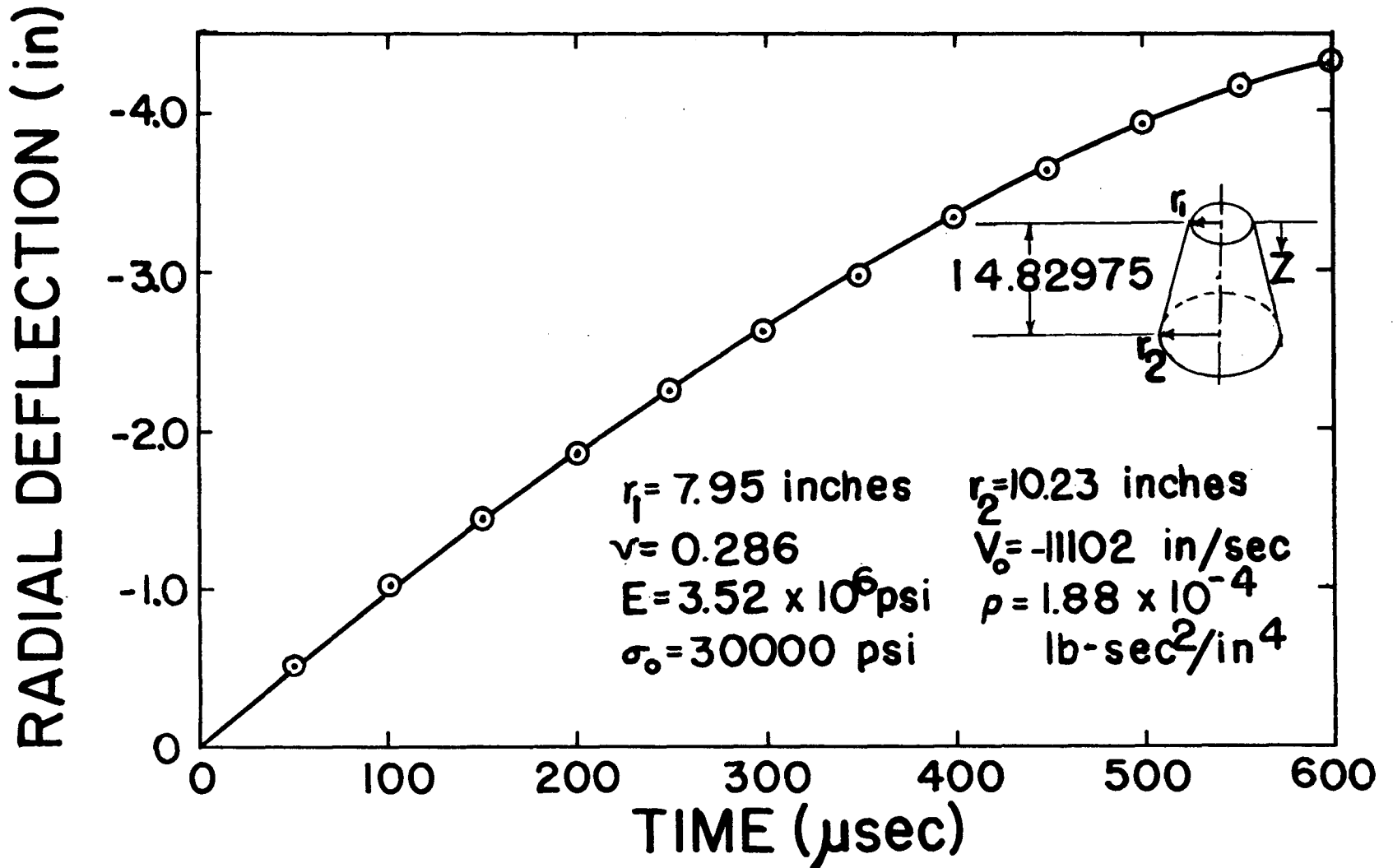


FIG.21 RADIAL DEFLECTION AT THETA = 0.0° AND Z = 6.3516 in

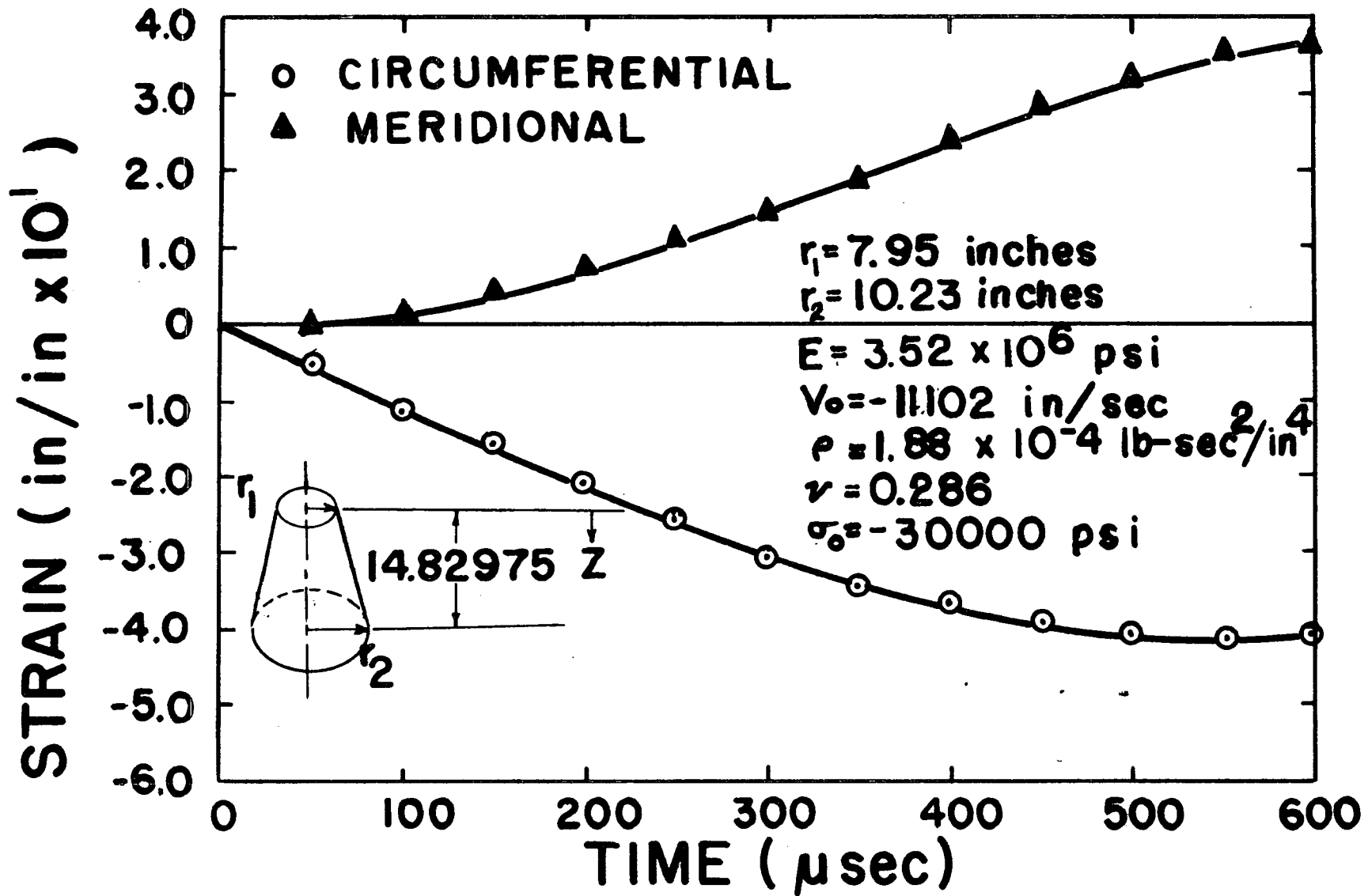


FIG. 22 MERIDIONAL AND CIRCUMERENTIAL STRAIN
 AT THETA=0 AND Z=6.3516 inches
 (INNER SURFACE)

20

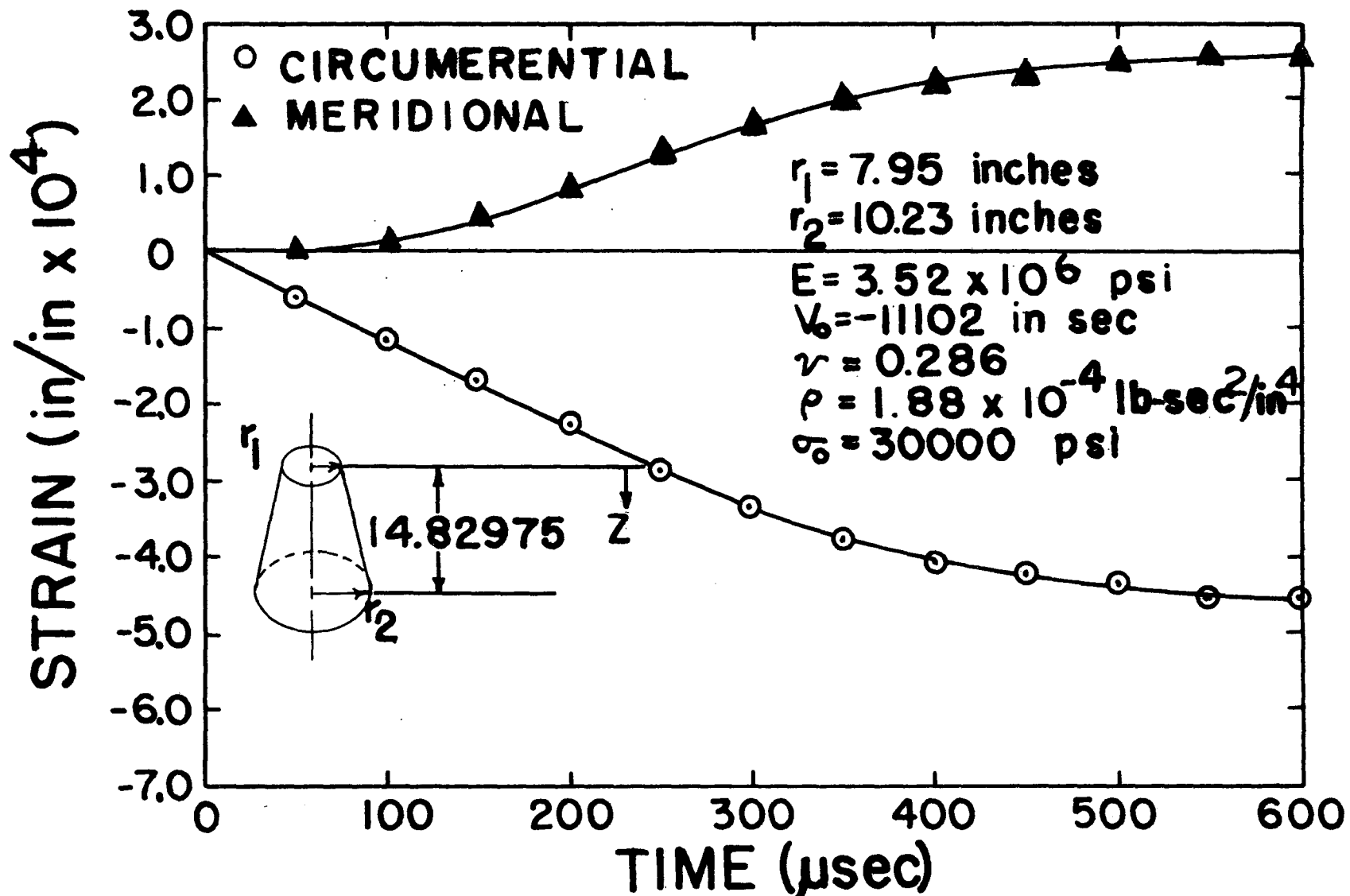
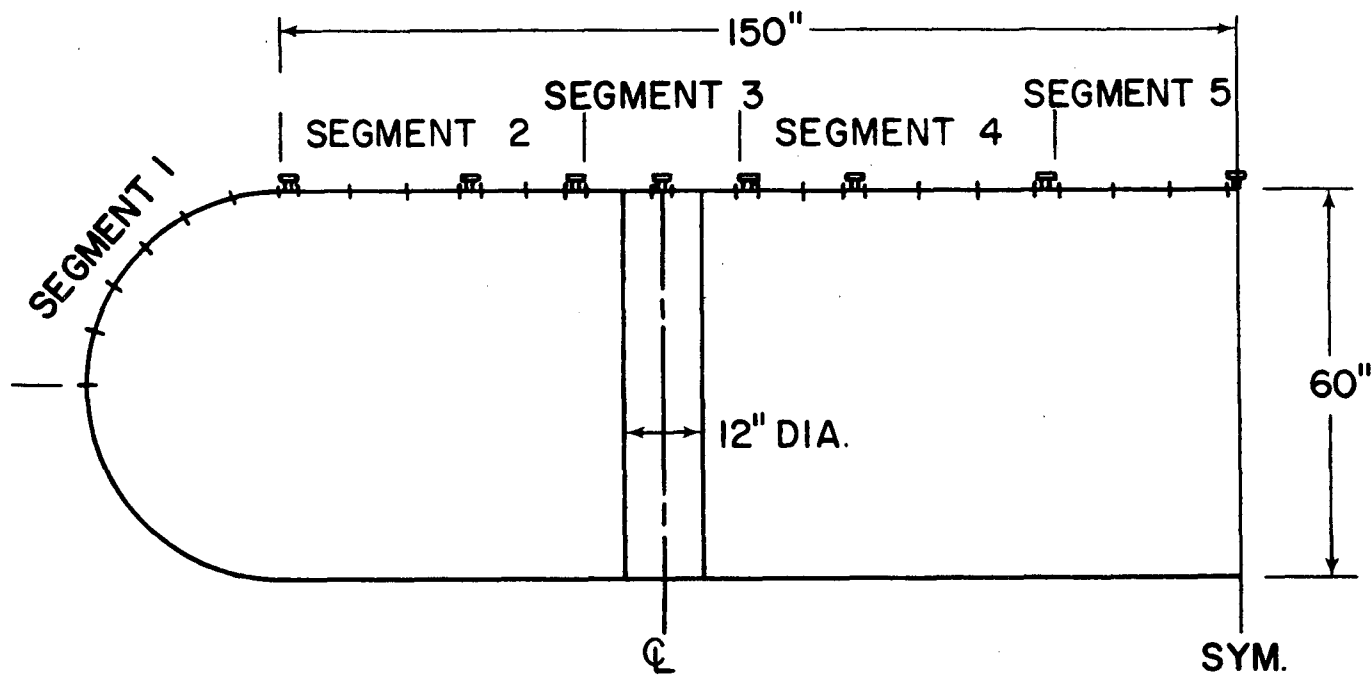
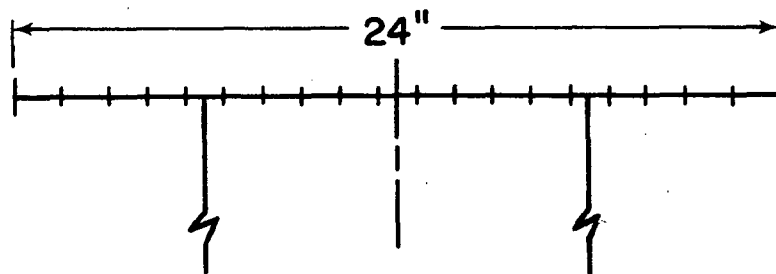


FIG.23 MERIDIONAL AND CIRCUMFERENTIAL STRAIN
 AT THETA = 00° AND Z = 6.3516 in (OUTER
 SURFACE)



(a) ELEMENT IDEALIZATION (SCALE: 1" = 30")



(b) SEGMENT 3 IDEALIZATION (SCALE: 1" = 6")

FIG. 25 ELEMENT IDEALIZATION OF STIFFENED SHELL

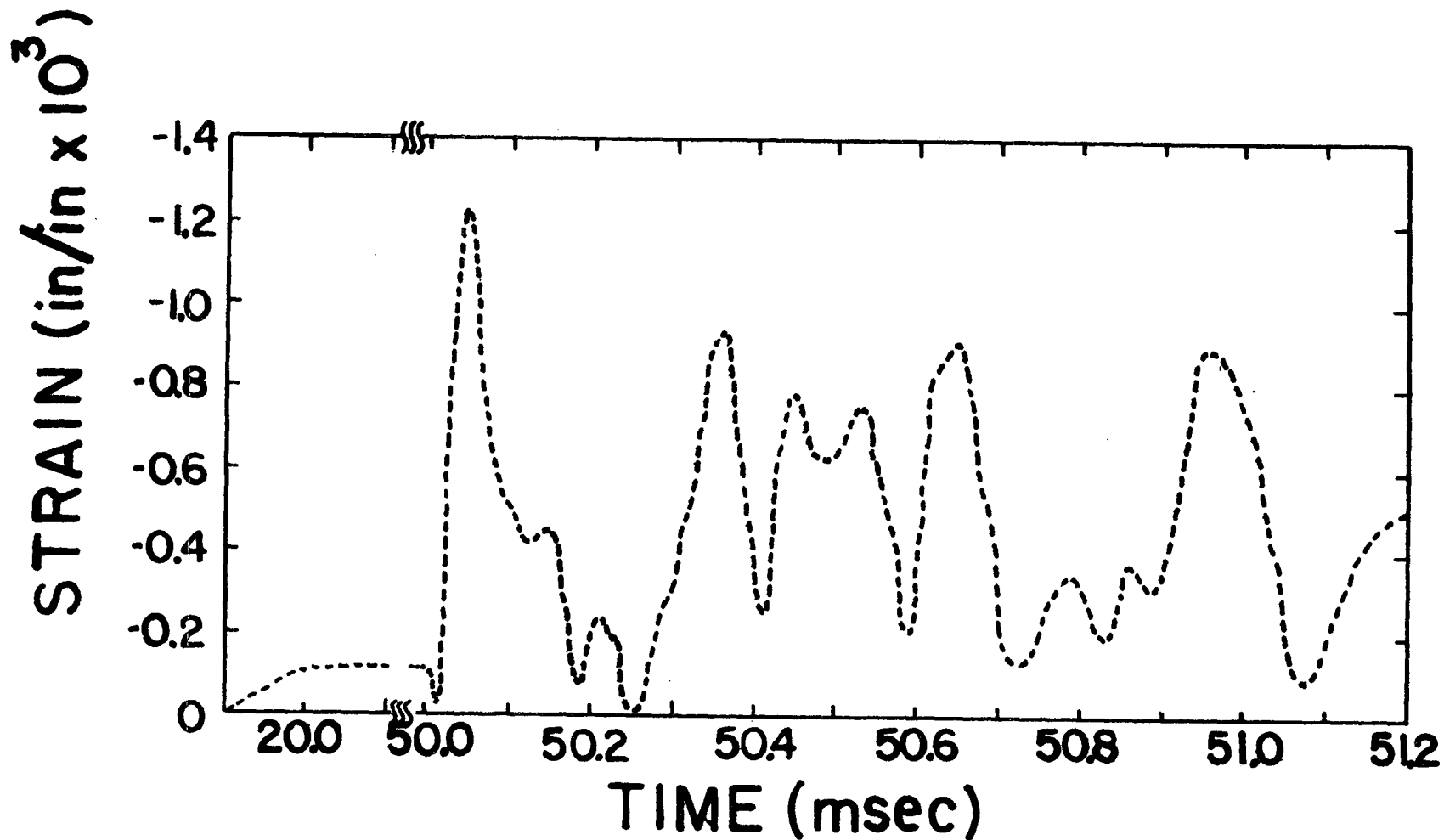
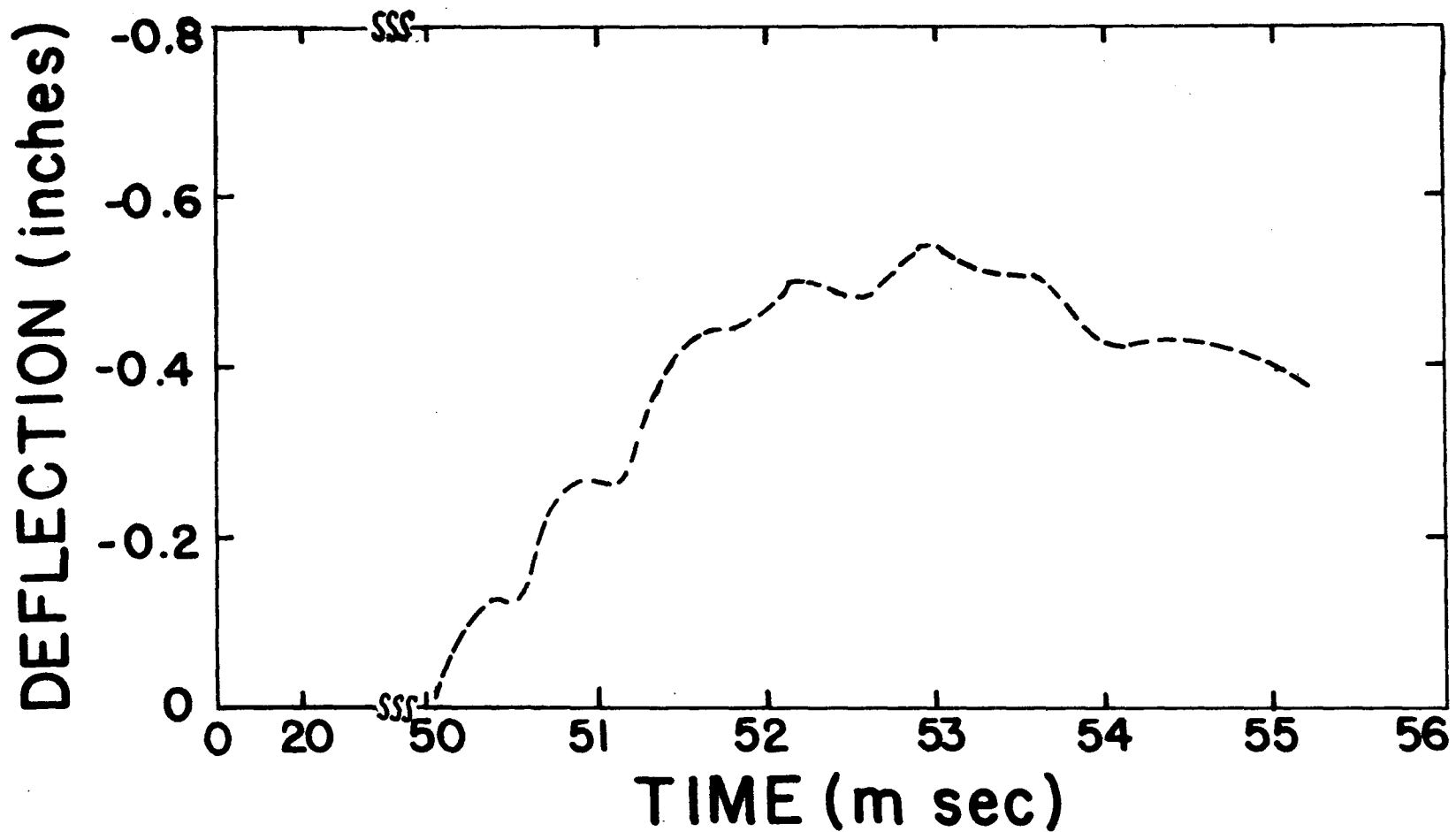


FIG.26 MERIDIONAL STRAIN AT THETA = 0.0°
AT VEHICLES' OUTER SURFACE



**FIG. 27 RADIAL DEFLECTION OF NODE 46
WITH RESPECT TO NODE 1 FOR
HARMONIC 1**

APPENDIX A

$$\frac{\partial \hat{e}_s}{\partial q_j} = \frac{\partial e_s^i}{\partial q_j} \cos i\theta$$

$$\frac{\partial \hat{e}_\theta}{\partial q_j} = \frac{\partial e_\theta^i}{\partial q_j} \cos i\theta$$

$$\frac{\partial \hat{e}_{s\theta}}{\partial q_j} = \frac{\partial e_{s\theta}^i}{\partial q_j} \sin i\theta$$

$$\frac{\partial \hat{e}_{13}}{\partial q_j} = \frac{\partial e_{13}^i}{\partial q_j} \cos i\theta$$

$$\frac{\partial \hat{e}_{23}}{\partial q_j} = \frac{\partial e_{23}^i}{\partial q_j} \sin i\theta$$

$$\frac{\partial \kappa_s}{\partial q_j} = \frac{\partial^2 e_{13}^i}{\partial s \partial q_j} \cos i\theta$$

$$\frac{\partial \kappa_\theta}{\partial q_j} = -\frac{1}{r} \left[\frac{\partial^2 e_{23}^i}{\partial \theta \partial q_j} \sin i\theta + \frac{\partial e_{13}^i}{\partial q_j} \cos i\theta \sin \phi \right]$$

$$\frac{\partial \kappa_{s\theta}}{\partial q_j} = \frac{1}{r} \left[-\frac{\partial^2 e_{13}^i}{\partial \theta \partial q_j} \cos i\theta + \frac{\partial e_{23}^i}{\partial q_j} \sin i\theta \sin \phi \right] - \frac{\partial^2 e_{23}^i}{\partial s \partial q_j} \sin i\theta$$

No summation on i

$$\frac{\partial e_\theta}{\partial q_3} = \frac{1}{2r}$$

$$\frac{\partial e_{\theta}}{\partial q_7} = \frac{1}{2r}$$

$$\frac{\partial e_{23}}{\partial q_2} = -\frac{\cos \phi}{2r}$$

$$\frac{\partial e_{23}}{\partial q_6} = \frac{\partial e_{23}}{\partial q_2}$$

$$\frac{\partial e_{13}}{\partial q_1} = \frac{\sin \phi}{s}$$

$$\frac{\partial e_{13}}{\partial q_3} = -\frac{\cos \phi}{s}$$

$$\frac{\partial e_{13}}{\partial q_5} = -\frac{\partial e_{13}}{\partial q_1}$$

$$\frac{\partial e_{13}}{\partial q_7} = \frac{\partial e_{13}}{\partial q_3}$$

$$\frac{\partial e_{s\theta}}{\partial q_2} = -\frac{\sin \phi}{2r} - \frac{1}{s}$$

$$\frac{\partial e_{s\theta}}{\partial q_6} = \frac{\sin \phi}{2r} + \frac{1}{s}$$

$$\frac{\partial e_s}{\partial q_1} = \frac{\partial e_{13}}{\partial q_3}$$

$$\frac{\partial e_s}{\partial q_3} = \frac{\partial e_{13}}{\partial q_1}$$

$$\frac{\partial e_s}{\partial q_5} = \frac{\partial e_{13}}{\partial q_7}$$

$$\frac{\partial e_s}{\partial q_7} = \frac{\partial e_{13}}{\partial q_5}$$

$$\frac{\partial \kappa_s}{\partial q_4} = \frac{1}{s}$$

$$\frac{\partial \kappa_s}{\partial q_8} = -\frac{1}{s}$$

$$\frac{\partial \kappa_{s\theta}}{\partial q_2} = -\frac{\cos \phi}{rs} + \frac{2 \sin \phi}{r} \frac{\partial e_{23}}{\partial q_2}$$

$$\frac{\partial \kappa_{s\theta}}{\partial q_6} = \frac{\cos \phi}{rs} + \frac{2 \sin \phi}{r} \frac{\partial e_{23}}{\partial q_6}$$

The following partial derivatives are a function of the harmonic number i .

$$\frac{\partial e_{23}^i}{\partial q_1^i} = \frac{i \sin \phi}{2r}$$

$$\frac{\partial e_{23}^i}{\partial q_3^i} = -\frac{i \cos \phi}{2r}$$

$$\frac{\partial e_{23}^i}{\partial q_5^i} = \frac{\partial e_{23}^i}{\partial q_1^i}$$

$$\frac{\partial e_{23}^i}{\partial q_7^i} = \frac{\partial e_{23}^i}{\partial q_3^i}$$

$$\frac{\partial e_{s\theta}^i}{\partial q_1^i} = \frac{\partial e_{23}^i}{\partial q_3^i}$$

$$\frac{\partial e_{s\theta}^i}{\partial q_3^i} = \frac{\partial e_{23}^i}{\partial q_1^i}$$

$$\frac{\partial e_{s\theta}^i}{\partial q_5} = \frac{\partial e_{23}^i}{\partial q_7}$$

$$\frac{\partial e_{s\theta}^i}{\partial q_7} = - \frac{\partial e_{23}^i}{\partial q_5}$$

$$\frac{\partial e_{\theta}^i}{\partial q_2} = \frac{i}{2r}$$

$$\frac{\partial e_{\theta}^i}{\partial q_6} = \frac{\partial e_{\theta}^i}{\partial q_2}$$

$$\frac{\partial \kappa_{\theta}^i}{\partial q_1} = - \frac{i}{r} \frac{\partial e_{23}^i}{\partial q_1} - \frac{\sin \phi}{r} \frac{\partial e_{13}}{\partial q_1}$$

$$\frac{\partial \kappa_{\theta}^i}{\partial q_2} = - \frac{i}{r} \frac{\partial e_{23}^i}{\partial q_2}$$

$$\frac{\partial \kappa_{\theta}^i}{\partial q_3} = - \frac{i}{r} \frac{\partial e_{23}^i}{\partial q_3} - \frac{\sin \phi}{r} \frac{\partial e_{13}}{\partial q_3}$$

$$\frac{\partial \kappa_{\theta}^i}{\partial q_5} = - \frac{i}{r} \frac{\partial e_{23}^i}{\partial q_5} - \frac{\sin \phi}{r} \frac{\partial e_{13}}{\partial q_5}$$

$$\frac{\partial \kappa_{\theta}^i}{\partial q_6} = - \frac{i}{r} \frac{\partial e_{23}^i}{\partial q_6}$$

$$\frac{\partial \kappa_{\theta}^i}{\partial q_7} = - \frac{i}{r} \frac{\partial e_{23}^i}{\partial q_7} - \frac{\sin \phi}{r} \frac{\partial e_{13}}{\partial q_7}$$

$$\frac{\partial \kappa_{s\theta}^i}{\partial q_1} = \frac{2i}{r} \frac{\partial e_{13}}{\partial q_1} + \frac{2 \sin \phi}{r} \frac{\partial e_{23}^i}{\partial q_1}$$

$$\frac{\partial \kappa_{s\theta}^i}{\partial q_3} = \frac{2i}{r} \frac{\partial e_{13}}{\partial q_3} + \frac{2 \sin \phi}{r} \frac{\partial e_{23}^i}{\partial q_3}$$

$$\frac{\partial \kappa_{s\theta}^i}{\partial q_5} = \frac{2i}{r} \frac{\partial e_{13}}{\partial q_5} + \frac{2 \sin \phi}{r} \frac{\partial e_{23}^i}{\partial q_5}$$

$$\frac{\partial \kappa_{s\theta}^i}{\partial q_7} = \frac{2i}{r} \frac{\partial e_{13}}{\partial q_7} + \frac{2 \sin \phi}{r} \frac{\partial e_{23}^i}{\partial q_7}$$

All other partial derivatives are equal to zero.